# Infrared thermography for quantitative thermal performance assessment of wood-framed building envelopes in Canada

Milad Mahmoodzadeh [a], Voytek Gretka [b], Ivan Lee [c], Phalguni Mukhopadhyaya [a],*

[a] *Department of Civil Engineering, University of Victoria, Victoria, BC V8W 2Y2, Canada*
[b] *Department of Building Specialty Services, Morrison Hershfield Ltd., Victoria, BC V8W 1C6, Canada*
[c] *Department of Building Specialty Services, Morrison Hershfield Ltd., Vancouver, BC V5C 6S7, Canada*

## ARTICLE INFO

## ABSTRACT

Since many buildings in Canada were built prior to the advent of national and provincial energy codes and standards, quantifying building envelope thermal performance is an important step in identifying retrofit opportunities in existing buildings. This study aimed to use external quantitative infrared thermography (IRT) to estimate effective U-value of opaque building envelopes (considering the effect of thermal bridging sources) of a conditioned at-scale structure comprised of four wood-framed wall assemblies commonly used in Canada. Furthermore, the effect of vignetting artefacts on effective U-value measurements was assessed, followed by a practical approach to correcting for it to improve accuracy of U-value estimation and calibration of energy models. Additionally, a comprehensive uncertainty analysis was performed to evaluate the impact of input variables on the accuracy and uncertainty of results. Finally, apart from qualitative and quantitative thermal assessment of the building envelope, a novel relative quantitative infrared index (IRI) methodology was proposed as a means to facilitate rapid evaluation and subsequent ranking of building envelope thermal performance. The results indicated that vignetting effect has an adverse impact on the accuracy of results, in particular for well-insulated walls where deviations of $-42.31\%$ to $-83.33\%$ were observed. However, when the proposed practical approach was implemented, substantial improvements in accuracy of walls' U-value were obtained, ranging from $-2.33\%$ to $-12.50\%$ after correction versus $-13.95\%$ to $-58.33\%$ without correction. Moreover, the results indicated that the energy model was substantially more accurate when the effect of thermal bridges were accounted for, and the adverse effect of vignetting was addressed in the estimation of U-value. In this case, ASHRAE Guideline 14 criteria were satisfied: Normalized Mean Bias Error (NMBE) < 5%, and Coefficient of Variation of the Root Mean Square Error (CVRMSE) < 15%. The findings of the uncertainty budget demonstrated that the influence of parameters on U-value depends on the type of wall assembly. Ultimately, wall thermal performance rankings based on IRI were consistent with their U-value rankings, implying that IRI can be a reliable metric for relative quantitative comparison of building envelope thermal performance, regardless of boundary conditions.

© 2021 Published by Elsevier B.V.

## 1. Introduction

Globally, space heating and cooling accounts for over one-third of overall energy consumptions in buildings. With a revived concern for building energy consumption, aggressive energy conservation policies have been adopted at national and regional levels. For instance, the province of British Columbia, and later Canada, committed to reduced net greenhouse emissions by 80% of 2007 and 2005 levels, respectively, by 2050 [1–2], as have been adopted by other G7 nations at the recent Paris Climate Summit [3]. In the wake of these policies, building certifications through energy audits are becoming a common means of grading energy performance, and in part the overall building sustainability. Since existing buildings in Canada are predicted to account for almost half of total building stock by 2050, Canadian policymakers are gradually focus on improving the energy use intensity (EUI) of these buildings [4].

One of the most critical considerations in a building energy assessment is the thermal performance of the building envelope. It is evident that with more heat transfer through the building

* Corresponding author.
*E-mail addresses:* miladmahmoodzadeh@uvic.ca (M. Mahmoodzadeh), vgretka@morrisonhershfield.com (V. Gretka), ilee@morrisonhershfield.com (I. Lee), phalguni@uvic.ca (P. Mukhopadhyaya).

envelope, a greater amount of energy needs to be consumed to maintain a similar indoor air temperature [5]. IEA's technology roadmap for energy-efficient buildings indicated that improving the thermal performance of the building envelope can lead to an energy use reduction of 57% and 42% in commercial and residential buildings, respectively [6]. To this end, researchers worldwide have conducted various studies to evaluate the impact of the building envelope on building energy performance. For instance, Osma et al. [7] considered different retrofit design strategies to achieve a net-zero energy performance of a university building in Tripoli, Lebanon. It was found that by retrofitting the building envelope through upgrading the walls and floor with additional insulation, the EUI of a building can be reduced by 28%, which was more effective than upgrading HVAC and lighting systems. Lin et al. [8] showed that optimizing the thermal performance of building envelope of office buildings in Taiwan can save almost 41% of energy costs. Elsewhere, Balaras et al. [9] indicated that the energy consumption of well-insulated apartment buildings in Greece was 20–40% less than non-insulated buildings. It can be deduced that identifying the actual thermal performance of building envelopes is essential to understand any potential opportunities for improvement.

Currently, a detailed energy assessment of a building is performed with simulation tools. Achieving accurate results requires reasonably accurate inputs such as climate data, building envelope thermal properties, internal load profiles (lighting, equipment, levels of activity, …), air leakage rates, type of mechanical systems, and occupant behaviour. Uncertainties in input values can adversely affect the selection of appropriate retrofit strategies [10]. One of the most uncertain inputs in energy models is the building envelope's thermal characteristics, which are mainly applied in models based on design values obtained from reference tables. However, the actual U-value of the building envelope differs from its design due to the ageing of insulation materials, variation of materials moisture content, quality of installation, structural defects (cracks; voids), and fluctuation of external conditions such as temperature, humidity, solar radiation and precipitation [10–11]. For instance, the Italian Standard UNI 10,351 reported differences of 5% to 50% between the field and lab measurements of material thermal conductivity [12]. Similarly, Evangelisti et al. [13] through a study using a heat flow meter in a lab environment, concluded that deviations between theoretical and measured U-values of wall assemblies can be as high as 153%. Therefore, in-situ quantification of building envelope thermal performance is required to reduce the uncertainties in energy modelling results, and inform implementation of the most appropriate energy conservation measures (ECMs) [12].

In the last few decades, non-destructive testing techniques such as heat flux meters (HFMs) and infrared thermography (IRT) have become prominent tools for on-site assessments of building envelope thermal performance [14]. However, HFMs are only a point source measurement that ignores the impact of thermal bridges or material irregularities, ultimately limiting its effectiveness as a data collection technique for spreadsheet-based energy audits or dynamic whole-building energy modelling. Furthermore, measurements require a minimum test duration of 72 h (at least 96 h for materials with high specific heat capacities), which is often not practical for practitioners; in this context, IRT has drawn attention as a viable alternative [14].

IRT is a non-destructive tool that determines the temperature of objects based on the radiation emitted from the object's surface. Traditionally, IRT has been used mainly for military purposes [15–16], medical applications such as visualizing the early stages of breast cancer [17], identifying the hot spots during the inspection of high-voltage power lines [15,17], and inspections of HVAC and electric systems in buildings [18]. By the early 2000 s, the

application of IRT was expanded as a means to identify thermal irregularities for energy audit purposes in buildings [19]. Following this, International standards such as ISO 6781:1983 [20], UNE EN 13187:1998 [21], ASTM E1311 [22], ASTM E1862 [23], and guidelines (i.e., RESNET [24]) have established required boundary conditions and procedures for the use of qualitative IRT in the energy audits of buildings, to ensure reliable and comparable results. Nevertheless, many authors have recently attempted to develop an accurate approach for estimating the in-situ U-value of building envelope using quantitative IRT [25–32].

Decreasing costs and improved portability of infrared cameras with the ability to connect to smartphones have collectively provided opportunities for energy advisors, homeowners, and property managers to observe temperature anomalies in thermal images. The widespread accessibility of this technology implies it could eventually be a ubiquitous inspection tool that helps inform building envelope retrofit strategies for the purposes of energy efficiency [33].

Although the majority of studies were conducted in European countries [26–31], this research aims to provide some insights into how quantitative IRT can evaluate thermal performance of wood-framed wall assemblies in Canada in the context of local construction practices and building codes. This paper consists of three main sections: 1) background, which provides an overview of recent applied methodologies in the evaluation of building envelopes using IRT; 2) methodology, which describes how the wall assemblies of a simple one-zone structure were assessed, outlines data collection procedures, followed by the development of a dynamic whole-building energy model of the structure to examine the feasibility of using external IRT in calibrating energy simulation models; 3) results, which summarizes findings from the IRT measurement and the calibration of the simulated model, and; 4) conclusion, that highlights the major contribution of this research and potential next steps in refining the techniques herein for utilization by practitioners.

## 2. Background

Over the last 25 years, IRT has been widely utilized in the inspection of building envelope physical deterioration [10]. Most building envelope defects are ultimately a result of moisture accumulation, which can occur either by poor envelope detailing allowing precipitation ingress from the exterior, or by via condensation at locations with thermal bridging from air leakage [34]. However, thermal patterns associated with either scenario are different, which are important to identify. For instance, moisture or pooling water within the building envelope presents as a non-homogenous thermal pattern on the surfaces, often reducing the measured temperature due to evaporative cooling. Areas with thermal bridging have a higher pixel intensity compared to undisturbed areas when analyzed with external IRT, in general. Likewise, hot spots in building envelope due to the degradation/missing of thermal insulation or air leakage effects are detectable by IRT. These anomalies in thermal behavior of building components are mainly determined with qualitative IRT, while quantification of thermal irregularities and assessment of insulation thermal performance require quantitative methods [34]. Generally, in both quantitative and qualitative approaches, anomalies on the surface are evaluated visually or numerically based on their temperature patterns in thermal images (explained further in the following subsections).

### 2.1. Qualitative IRT

Qualitative IRT is widely adopted in building inspections to obtain a variety of information. For example, it is used to identify

sources of air leakage, locations of thermal bridging, trapped moisture and water, thermal insulation discontinuity, performance of HVAC and electrical systems after installation such as detection of air and water leakage from pipes and ducts, insulation of distribution ducts and pipes, failure in bearing, lubrication and/or electrical motors (hot spots due to the mechanical stress), thermal comfort assessment by visualizing variations in skin temperature on different parts of a human face, and measurement of indoor and surface temperatures [19]. Irregularities can be quickly interpreted based on colour patterns and intensity differences in thermal images. In other words, qualitative IRT determines the anomalies, but it does not necessarily inform about the severity of defects [34].

A range of studies have been conducted to assess the performance of building envelope assemblies using qualitative thermography. For instance, a study on a historical building was undertaken to analyze earthquake damage using qualitative IRT [35]. Images showed locations of thermal anomalies after the earthquake, leading the authors to conclude that qualitative IRT was a useful technique to advise safety precautions for historical building renovations. Goodhew et al. [36] conducted a study to assess the heat losses of ten houses in the UK using qualitative IRT. Psychological reactions of household members after the thermographic survey were recorded, in particular their tendencies to adopt energy-saving behaviours. The results revealed that the outcomes of qualitative surveys were satisfying for each individual and motivated them to apply energy conservation measures (ECMs). A thermographic survey was conducted by Ocana et al. [37] on two different buildings (modern vs. historical) in Spanish rural areas to evaluate the usefulness of IRT in thermal assessment of rural buildings. The surveys were performed at two times, one in the late evening and the other in the early morning. IRT results indicated that for modern building whose walls were non-load bearing and relatively thin, the best results were obtained during the daybreak inspection. However, for the inspection of traditional building which had thicker walls with high thermal inertia, IRT provided better results during the evening inspection. Mahmoodzadeh et al. [38] combined IRT with a blower door test to determine the minimum required pressure difference for detecting sources of air leakage around a window frame. It was found that a minimum pressure difference of 25 Pa is required to visualize the air leakage pattern with IRT at the window-to-wall interface as well as differentiate air leakage from a known thermal bridge (window frame). In addition, an IRT survey of 135 residential units in the Boston, MA metropolitan area indicated that heat losses through the windows, windows crack, chimney, and soffits were the dominant sources of heat loss, observed in almost 70% of buildings analyzed. Furthermore, to assess the contribution of heat transfer modes in energy losses, it was found that on a heated residential building, air leakage through cracks (windows & doors) and ducts account for nearly 40% of total energy losses, and conduction heat transfer through the walls and windows account for the other 40% of energy lost. This provided a simplified framework to identify which sources should be focused to reduce the energy losses in buildings [39]. Given these findings, it can be inferred that qualitative IRT can be a reliable method for the identification of building envelope defects and thermal bridges. When used in an energy audit setting, it can help homeowners and property managers implement targeted, cost-effective envelope retrofits [34].

### 2.2. Relative quantitative IRT

Building envelope retrofits are typically performed when its physical condition at the end of its service life, aesthetic (vintage), or the building energy use intensity (EUI) dictates it is required [40]. In the case of a portfolio or campus of buildings under the purview of a single property manager, prioritizing envelope retrofits is not a straightforward exercise. Compiling building-level envelope data is time-consuming, while global approximations that are applied to the whole portfolio may lack enough accuracy to inform conclusions about relative energy performance [40]. For instance, Mahmoodzadeh et al. [40] showed that the rank of buildings based on a single criterion such as age and physical condition yielded different results, with no correlation to overall heat loss (UA) through the building envelope. While qualitative IRT demonstrated a robust method for determining the thermal anomalies and visualizing their thermal patterns, a metric for identification and prioritization of thermal anomalies in the building envelope is required. To this end, researchers have used the concept of Temperature Index (TI), which is defined as the ratio of the temperature difference between the interior surface and outdoor air to the temperature difference between the indoor and outdoor air (assuming one-dimensional heat transfer and steady state conditions). TI has been used to determine and prioritize the thermal irregularities in building envelope such as thermal bridges, condensation, mould growth, and air leakage. For instance, the International Energy Agency (IEA) has proposed to use TI as a metric to assess relative impacts of thermal bridges [41]. Similarly, the Building Envelope Thermal Bridging Guide (BETB) has applied the concept of TI to determine potential areas of condensation risk due to the effect of thermal bridging in building components [42]. Ilomets et al. [43] used TI for a critical analysis of thermal bridging sources and probability of failure in six dwelling units before renovation. To this end, IRT was used to measure the temperature of internal surfaces at different points and TIs were measured accordingly. The results indicated that the risk of surface condensation due to thermal bridging was 51% in concrete buildings and almost 50% for wood and brick buildings. However, the probability of mould growth in the concrete building was determined to be 54% compared to 46% and 45% in wood and brick buildings, respectively. Additionally, many countries have established various TI design values to assess condensation in the building envelope. For example, TI should be at least 0.75 for dwellings in the United Kingdom to avoid moisture damage and surface condensation [44]. Similarly, Dutch building regulations set the minimum TI of 0.65 for new residential buildings [45]. Finland recommended a TI of 0.97 for floors, 0.87 for walls, and 0.65 at the junction of the external walls. Several other studies have used TI to determine sources of air leakage [46]; for instance, Kalamees [47] studied houses in Estonia and found that ceiling/floor-wall, window-wall, and interior/exterior wall-roof interfaces were the main sources of air leakage. Similarly, Mahmoodzadeh et al. [38] used TI as a metric to identify sources of air infiltration around an interior window frame by depressurizing the surrounding room.

In the aforementioned investigations, TI was obtained using internal IRT based on the surface temperature of spots around the areas of thermal anomalies to infer potential conclusions about the building envelope thermal performance. However, in practice, internal IRT may disturb building programming (occupant activities) and is a cumbersome procedure. Furthermore, temperature measurement based on spots informs only the relative comparison of a particular thermal anomaly at different areas and does not indicate the overall thermal performance of a building envelope assembly compared to others. Hence, a rapid metric (i.e., index) which considers the overall impact of all sources of heat losses such as an opaque wall, windows, doors, thermal bridge, air leakage, and defects (entire surface of an envelope) based on external IRT is required for relative quantitative comparison of the entire building envelope. It should be noted that the development of a ranking metric could serve as a good indicator for policymakers, homeowners, home inspectors, and property managers to compare thermal performance of building envelope assemblies of various

buildings on a regional or portfolio scale for prioritization of energy retrofit strategies.

### 2.3. Quantitative IRT

In the hopes of creating less invasive and more accurate quantitative measurements, researchers have developed methodologies that utilize infrared cameras as a means of data collection to quantify thermal anomalies, measure in-situ U-value, determine dynamic characterization of building elements, estimate linear thermal transmittance (psi-value), evaluate insulation effectiveness, and identify moisture ingress [19]. These methodologies study the subject under in-situ conditions (passive thermography), in contrast to active thermography which utilizes an external thermal stimulus [48]. Passive thermography has the advantage in that it can be employed to inspect the entirety of the building envelope quickly and has also shown promise as a potential candidate for automation [49].

IRT surveys are performed both from the interior and exterior; typically indoor IRT results are more acceptable than external IRT due to reduced climatic fluctuations and unknown thermal reflections from the surroundings, and relatively mitigated air movement implying a only minor variations in convective heat transfer coefficient [11,19,33]. Theoretical and measured U-values have been shown to deviate between 10 and 60% for external thermography compared to a range of only 2–12% for internal thermography [33]. Danielski and Fröling [50] also demonstrated an improved indoor infrared thermography method for determining U-values that produced results with only a 4% difference from standardized HFM measurements, suggesting that the two methods could be equally effective in 1-D measurements, and that the thermography approach is more appropriate given its ability to record measurements of the entire wall segments (2-D) yielding more representative results. However, Dall'O' et al. [28] and Albatici et al. [29] stated that the deviation between measured data and theoretical values in external IRT could exceed 50%, depending on wind speed and assembly construction. Although the stability of indoor conditions in indoor IRT can help practitioners obtain more precise results, current methodologies in literature suggest it is possible to estimate the U-value of a building element, and in turn estimate heat loss through it utilizing an external thermographic survey and accompanying internal temperature measurement of the walls' surface or internal air temperature. This leads to the potential of creating a strictly external thermographic survey methodology auditing the entire building envelope in a short period of time. Consequently, development of this kind of external IRT technique facilitates future utilization of unmanned aerial vehicles (UAVs) equipped with infrared cameras for conducting large-scale quantitative surveys in a fraction of the time without the need for current intrusive methods.

Currently, infrared camera technology touts temperature sensitivity as low as 30mK, which is often misinterpreted as the accuracy of the surface temperature estimate produced by the system as a colourized image. Thermographic sensors have built-in computers that interpret the signal received as a temperature using a simple radiometric model based on the subject's emissivity, the surrounding ambient temperature reflected off the Gray Body subject, and the subject's emitted radiation [51–54]. These parameters have been shown to greatly influence the temperature estimate, and if not properly measured and compensated for, can result in an error in estimated U-value on the order of 100% due to a surface temperature measurement error of only 1°-3°K [26,31]. Additionally, environmental parameters such as solar irradiation, sky condition, wind, and moisture could have a substantial effect on the accuracy of thermographic readings. Recently conducted studies have led to the establishment of a handful of best practices for

thermographic surveys to improve the accuracy of results by reducing noise [19,55–56]. Recommended solutions to obtain more reliable data are 1) performing the tests in stable weather [28–29,57]; (2) avoiding IRT surveys during rainy and sunny days [14,29]; (3) calculating the convective heat transfer coefficient based on average wind speed [28,58]; (4) considering compensation parameters such as emissivity and reflected temperature (i.e., the apparent temperature of surrounding objects that are reflected off the target into the infrared thermography camera) [26–29]; (5) using the IR camera to measure surface, indoor and outdoor temperature to minimize the systematic error [29,59] ; (6) conducting a sensitivity analysis to analyze the impact of radiation and boundary conditions on the results [26,28–29]; and (7) ensuring temperature differences of at least 10–15 K between the interior and exterior to allow sufficient heat flux through the element [26–29]. Moreover, it was suggested to select the region of interest (ROI) in the centre of thermal images due to profound vignetting artefacts, where temperature around the image perimeter appears colder than the actual surface temperature [59]. Furthermore, long-lasting surveys and averaged data were more reliable than short-term surveys due to a normalization of weather variations. In general, a short-term survey may not represent the actual performance of a building if the boundary conditions are not steady [19]. Due to these weather stability challenges, a number of research studies have measured U-value in controlled environments such as climate chambers or Guarded Hot Boxes [5,11,60].

A few investigations have devoted attention to the development of IRT methodologies to quantify the contribution of thermal bridges on measured U-values. In these studies, the variations in U-value due to thermal bridging were mainly determined based on the calculation of heat flux, linear thermal transmittance (psi-values) and incidence factor of thermal bridging [5,60–62]. The incidence factor is defined as the ratio between heat flux due to the influence of thermal bridging and the theoretical one-dimensional heat flux without thermal bridging [11,61]. The IRT methodology in these studies was based on an analysis of a line of pixels with and without a known thermal bridge. In other words, the contribution of thermal bridging to the deviation of U-value was based surface temperature of each pixel on a line selected by researchers [11,62]. Therefore, the 2D and 3D effect of thermal bridging were not necessarily accounted for. Building on these limitations, a few recent studies have attempted to quantify the 2D effect of thermal bridging in U-value measurements using IRT. For instance, Tejedor et al. [11] used internal IRT in a climate chamber to create a 2D U-value map for an entire façade of three common construction solutions in Southern European countries. The walls had different levels of thermal anomalies such as air void and gaps, defects with different depths, and large horizontal internal thermal bridges. The findings of this research facilitated a better and more accurate diagnosis of thermal bridging by measuring U-value at any point in the wall surface, as well as determining the average 2D U-value of facades by considering the effect of thermal anomalies. Mahmoodzadeh et al. [59] conducted an external IRT on three wood framed wall assemblies commonly found in buildings constructed in Canada to determine the U-value by considering the effect of repeated thermal bridging such as studs and attachment components. The U-values were determined by averaging the surface temperature of ROIs in thermal images, where the size of ROIs in the analysis closely corresponded to the size of simulated models (1220×813 mm). The results indicate measured U-values were comparable with the results of the 3D simulation, which differed by −11.53% to 10.00%. It was also concluded that due to the low level of lateral heat flux of wood framing (thermal bridging), external IRT could be a reliable method for quantification of U-values with thermal bridging in these wall assemblies.

Although the 2D effect of thermal bridging was identified in previous studies, in-situ measurements utilizing external IRT for the purposes of estimating overall U-value including all thermal bridging details (*effective* U-Value) such as intersections of wall-roof, window-wall, wall-floor, and corners is missing in literature. It should be noted that correct interoperation of thermograms requires an understanding of temperature distribution, test conditions and thermal image artefacts (ie. non-uniformity and vignetting) [59]. Therefore, employing external IRT in-situ to determine overall effective U-value requires further investigation.

The importance of estimating U-value in-situ from an energy perspective was also investigated by researchers. For instance, a study of 77 new buildings in Sweden showed that energy data was on average 20% higher than simulations suggested. It was found that this deviation can be explained by simulations that used design U-values rather than in-situ measurements (actual values) [50]. A study by Francis et al. [63] to evaluate the energy performance of dwellings with solid walls in the UK indicated that using assumed U-values instead of actual U-value can result in underestimation of annual space heating demand by 16%. A few recent studies have tried to incorporate the results of IRT into a building energy model to study the sensitivity of in-situ measurements on the accuracy of models. For instance, Bayomi et al. [10] conducted a survey with an infrared camera mounted on a UAV to determine the U-value of the building envelope for input to a building energy model. It was found that the goodness of fit, a statistical index defined by ASHRAE Research Procedure 1051 for evaluating the accuracy of simulation results, was improved from 21.8% to 0.9% for the calibrated energy model when the U-value determined by IRT was used. Benhmidou et al. [64] used the in-situ IRT U-value to simulate energy consumption of an existing building in Tangier (North of Morocco) and compared it with a reference model that used nominal U-values. The results showed that the reference model underestimated the energy consumption of the building, citing that heating and cooling loads were 44.47% and 48.21% lower than the model that used the in-situ U-value, respectively. It follows from literature that using IRT for energy model inputs can result in better estimation of building energy performance, and consequently more accurate conclusions about the economics of potential envelope retrofits. However, these studies neglected to account for the effect of all thermal bridging (*effective* U-value), which may result in substantial deviations in the accuracy of building energy models.

## 2.4. Problem statement and research objectives

The extensive literature review indicated that (1) qualitative IRT have been widely used to determine the source of thermal anomalies in building envelope, (2) the relative comparison of thermal irregularities severity in thermographic images were performed based on surface temperature of spots using temperature index, (3) quantitative IRT methodologies have been mainly performed to estimate U-value of a wall assembly without thermal bridging effects and how they compared with nominal design values, and (4) a few recent studies have attempted to quantify the contribution of thermal bridges in U-value measurement of wall assemblies in European construction practice using a climate chamber. However, it was found that in-situ estimation of effective U-value of a whole opaque wall using external IRT that comprehensively accounts for the effects of all thermal bridges (studs, wall-roof interface (parapet), window frame and corners) were not investigated yet. Also, previous studies have neither evaluated the effects of thermal imaging artefacts such as vignetting on the determination of U-value and its influence on the accuracy of building energy models, nor has a practical approach been developed to address or correct for this issue. Finally, quasi-quantitative comparisons of an entire building's vertical envelope thermal performance using external IRT has not been investigated.

To address the current gap in the literature, this study aims to assess the use of external IRT for determining the overall effective U-value of four insulated wood-framed wall assemblies typically found in Canada while introducing some practical techniques to improve the accuracy of measurements. U-values obtained with the IRT methodology are validated using the 3D finite element analysis software, Siemens NX [65]. Furthermore, the impact of estimated U-values on the accuracy of building energy models is examined. Finally, an infrared index (IRI) based on external IRT is introduced, as a metric that can help to rapidly evaluate and rank building envelope thermal performance. The findings of this research will help practitioners, energy auditors, and thermographers arrive at more sound conclusions. Fig. 1 below summarizes how IRT can be used in the context of the built environment.

3. Research method

## 2.5. Case study

The overall thermal transmittance coefficients measurement was carried out on a wood-framed test structure adjacent to an existing conditioned campus building at the University of Victoria, Victoria, BC, Canada. The structure was constructed on pier blocks instead of a typical foundation slab and has an area of 9.30 m² and a ceiling height of approximately 3.05 m. It consists of four different rain-screen wall assemblies (W1, W2, W3, and W4), shown in Fig. 2, which are representative of low-rise Canadian west-coast construction. The plan view and cross-section of the structure are available in Ref [59]. Highly insulated floor and roof assemblies (RSI-8.8) facilitate a better comparison of the different wall assemblies' thermal performance. An air gap of 19 mm exists behind the cladding due to mimic building code requirements for exterior walls in climate zones with high rain load, effectively improving drying potential of moisture that penetrates beyond the cladding. The components and material properties of the wall assemblies are described in Table 1.

W1, W2, W3, and W4 are facing East, North, South and West, respectively. Other than W1 which has an entrance door (2 m² & U = 2.5 W/m² K), other walls each incorporate a double-glazed window with fiberglass frame (0.16 m² & U = 1.59 W/m² K). It should be noted that W1 & W3 are facing the adjacent building while W2 and W4 are facing outdoor parking areas.

## 2.6. Measurement setup and data acquisition procedure

The equipment for this study included an IR camera, an oil-filled electric radiant heater, a metered power usage data logger, temperature sensors integrated with a data logger, and an anemometer to measure wind speed. All equipment was calibrated before the tests according to manufacturers' specifications. The infrared thermal camera model was a FLIR A65, with a 640 × 512 pixel focal plane array detector, 1.31 mrad geometric resolution, and a reported accuracy of 5 °C. Its spectral range was 7.5–13 μm, had a reported Noise Equivalent Temperature Difference (NETD) < 0.05 K at 30 °C, and had been calibrated against a blackbody by the manufacturer. Since the reported uncertainty of the IR camera by the manufacturer is based on lab conditions while this study is based on external IRT, the calibration of IR camera was further examined in outdoor environmental conditions by comparing the IRT measurement with a highly accurate temperature sensor. Accuracy of measurements with the IR camera were higher than those of the temperature sensor on average and were within the range of the camera's accuracy of 5 °C, confirming camera calibration. The calibration process is explained elsewhere by Mahmoodzadeh et al. [59].
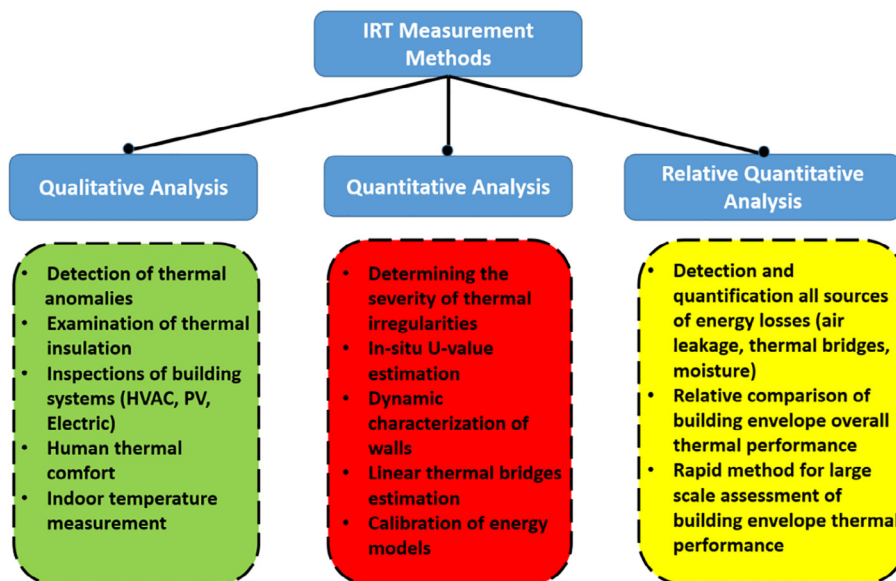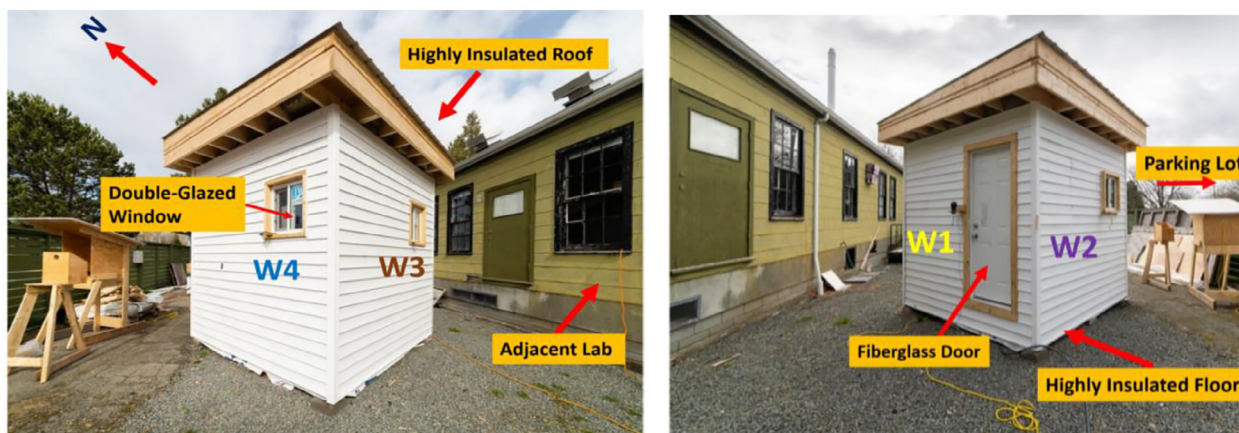
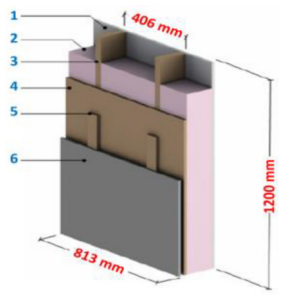**Fig. 1.** Application of IRT in buildings.



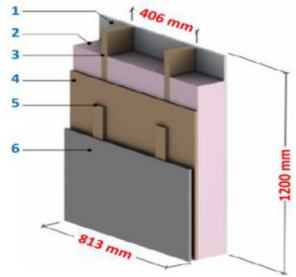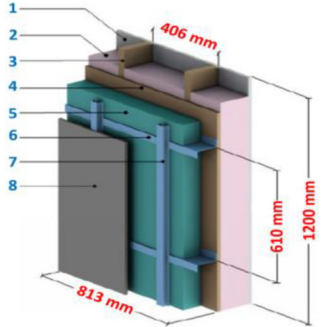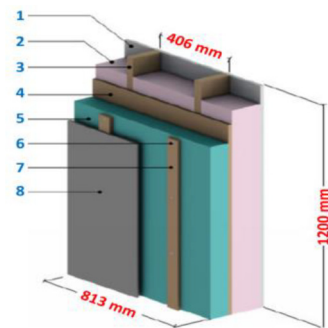**Fig. 2.** The experimental structure.

The structure is heated with the portable oil-filled electric radiant heater, and the total power usage associated with the heater was metered at 1-minute intervals. The surrounding environmental conditions were continuously monitored and recorded during and prior to the tests by data loggers, temperature sensors and anemometers. Since wind direction and intensity are not identical at different wall orientations, the wind speed for each wall was measured independently. An anemometer was positioned 1.5 m above grade and 0.1 m away from the wall exterior surface, and measured local wind speed in the vicinity of the exterior surface accurate to ± 0.1 m/s. Temperature sensors accurate to ± 0.01 °C and were positioned at different locations, both indoors and outdoors, to evaluate the variation of temperatures in the vicinity of the walls. To appreciate variations in indoor air temperature spatially, sensors were located at three different heights from the floor (0.5, 1.5, and 2.5 m) in three columns, forming a grid of 9 measurement locations [59].

Two criteria were considered in positioning the IR camera; (1) having the walls fully in the field of view, and (2) obtaining a minimum spot size ratio of 18 mm for detection of gross thermal patterns around insulation, thermal bridging components, and air leakage [59,66]. To this end, the IR camera was placed on a tripod

perpendicular at a distance of 5 m from the wall, achieving a spot size ratio of 6.5 mm (Fig. 3). Surveys were performed based on instantaneous IRT and weather conditions were quite stable thus steady-state conditions were reasonably approximated (cloudy sky, no precipitation, low wind speed < 1 m/s, and temperatures were constant). This allowed for U-value and infrared index of the walls to be comparatively analyzed, since boundary conditions were similar in all cases.

To validate the methodology, tests were performed on different days with varying exterior and interior conditions outlined in Table 2. Environmental factors such as solar radiation, wind speed, rain, sky conditions, and temperature gradient were monitored before and during the IRT surveys. The structure was not exposed to rain or snow 48 h prior to the tests and the sky was cloudy before (~12 h) and during the tests. Indoor air temperature was approximately constant before and during the tests (within ~ 2 °C tolerance of the thermostat deadband), and variations in outdoor temperature about 3–4 h prior the test were<0.5 °C and held constant during the tests. It should be noted that since the indoor temperature at different heights varied due to natural convection (stack effect), overall average indoor air temperature at the time of survey was considered and reported in Table 1. Relative

**Table 1**
Thermophysical properties of wall assemblies.

| Wall type | # | Component | Thickness (mm) | Conductivity (W/m K) | RSI-value (m² K/W) | 3D Sketch |
|---|---|---|---|---|---|---|
| **W1** | | Interior film | – | – | 0.12 | |
| | 1 | Gypsum Board | 13 | 0.16 | 0.08 | |
| | 2 | Fiberglass Batt Insulation | 89 | 0.036 | 2.47 | |
| | 3 | 2 × 4wood stud | 89 | 0.10 | – | |
| | 4 | Exterior plywood sheathing | 13 | 0.10 | 0.13 | |
| | 5 | 1 × 3wood strapping | 19 | 0.10 | – | |
| | 6 | Vinyl Cladding with 19 mm vented airspace incorporated into exterior heat transfer coefficient | | | | |
| | | Exterior film | – | – | 0.12 | |
| | | **Nominal RSI-value (m² K/W)** | **2.92** | | | |
| **W2** | | Interior film | – | – | 0.12 | |
| | 1 | Gypsum Board | 13 | 0.16 | 0.08 | |
| | 2 | Fiberglass Batt Insulation | 140 | 0.036 | 3.89 | |
| | 3 | 2 × 6wood stud | 140 | 0.10 | – | |
| | 4 | Exterior plywood sheathing | 13 | 0.10 | 0.13 | |
| | 5 | 1 × 3wood strapping | 19 | 0.10 | – | |
| | 6 | Vinyl Cladding with 19 mm vented airspace incorporated into exterior heat transfer coefficient | | | | |
| | | Exterior film | – | – | 0.12 | |
| | | **Nominal RSI-value (m² K/W)** | **4.34** | | | |
| **W3** | | Interior film | – | – | 0.12 | |
| | 1 | Gypsum Board | 13 | 0.16 | 0.08 | |
| | 2 | Fiberglass Batt Insulation | 140 | 0.036 | 3.89 | |
| | 3 | 2 × 6wood stud | 140 | 0.10 | – | |
| | 4 | Exterior plywood sheathing | 13 | 0.10 | 0.13 | |
| | 5 | Exterior insulation | 50 | 0.028 | 1.79 | |
| | 6 | Horizontal Z-Girt with 1 1/2″ Flange | 18 Gauge | 62 | – | |
| | 7 | Steel Furring Hat Track | 18 Gauge | 62 | – | |
| | 8 | Vinyl Cladding with 19 mm vented airspace incorporated into exterior heat transfer coefficient | | | | |
| | | Exterior film | – | – | 0.12 | |
| | | **Nominal RSI-value (m² K/W)** | **6.13** | | | |
| **W4** | | Interior film | – | – | 0.12 | |
| | 1 | Gypsum Board | 13 | 0.16 | 0.08 | |
| | 2 | Fiberglass Batt Insulation | 140 | 0.036 | 3.89 | |
| | 3 | 2 × 6wood stud | 140 | 0.10 | – | |
| | 4 | Exterior plywood sheathing | 13 | 0.10 | 0.13 | |
| | 5 | Exterior insulation | 50 | 0.028 | 1.79 | |
| | 6 | Wood strapping | 38 | 0.10 | – | |
| | 7 | #14 steel fastener | 11 | 50 | – | |
| | 8 | Vinyl Cladding with 19 mm vented airspace incorporated into exterior heat transfer coefficient | | | | |
| | | Exterior film | – | – | 0.12 | |
| | | **Nominal RSI-value (m² K/W)** | **6.13** | | | |

humidity was measured hourly at the local weather station (University of Victoria) which is made publicly available by the Government of Canada [67]. The average free stream wind speed during the day and during test were also recorded. The tests were performed in the late evening on an overcast night (almost 6 h after sunset) to minimize the effect of solar and night-sky radiation, and to minimize thermal mass effects. IR thermograms were recorded at 1-second intervals.

### 2.7. Surface temperature measurement

To obtain an accurate surface temperature measurement with an IR camera, accurate values of ambient air temperature, relative humidity, atmospheric transmittance ($\tau$), reflected apparent temperature, and emissivity should be determined during the post-processing of thermal images [68]. The atmospheric transmittance depends on infrared wavelength, the distance of the IR camera to the target, relative humidity and ambient air temperature. Infrared radiation that propagates through the air is absorbed by various particles such as $O_3$, $CO_2$, and $H_2O$. However, infrared energy absorption by the atmosphere varies by wavelength. For instance, wavelengths of 5-7$\mu m$ are almost entirely absorbed by the atmosphere. However, mid-wave (2-5$\mu m$) and long-wave (8-14$\mu m$) radiation is not well absorbed by the atmosphere, allowing more infrared energy to reach the sensor of the camera. Since the range of measured temperatures in this study was low (long-wavelength band), the absorption of long-wavelength radiation by IR camera is high considering the specifications of camera [68]. Furthermore, to incorporate the effect of atmosphere's temperature and relative humidity, and the effect of the distance between the target and
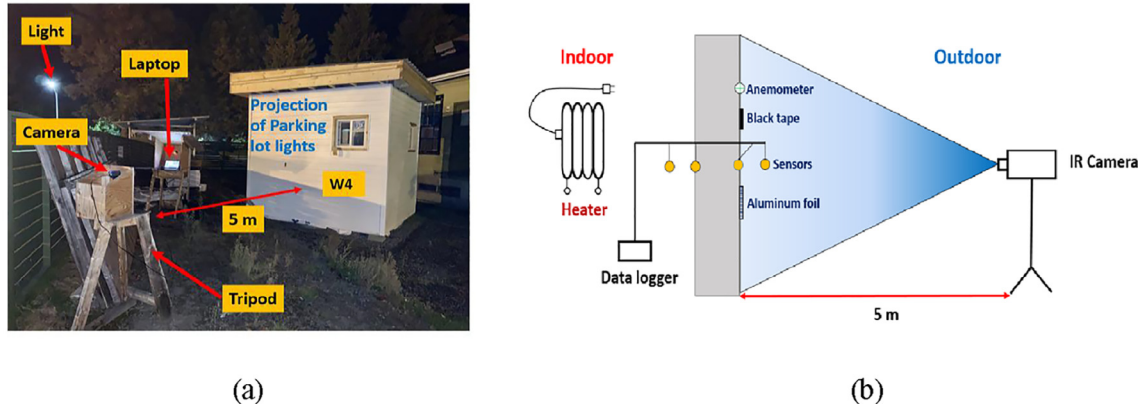
**Fig. 3.** Experimental set-up; (a) In-situ, (b) Schematic.

**Table 2**
Environmental conditions of tests.

| Boundary conditions | Day 1 | Day 2 | Day 3 | Day 4 | Day 5 |
|---|---|---|---|---|---|
| Outdoor Temperature (°C) | 5.50 | 6.22 | 7.00 | 4.61 | 3.13 |
| Outdoor air relative humidity (%) | 85 | 82 | 80 | 83 | 80 |
| Wind speed (m/s) | 0.31 | 0.23 | 0.10 | 0.12 | 0.71 |
| Sky condition | Cloudy | Cloudy | Cloudy | Cloudy | Cloudy |
| Average Indoor Air Temperature (°C) | 22.56 | 22.52 | 22.50 | 25.53 | 23.56 |

camera on atmospheric transmittance ($\tau$), the following formula was used by FLIR in the internal camera algorithm [69]:

$$\tau(d, w) = K_{atm}. \exp\left[-\sqrt{d}(\alpha_1 + \beta_1\sqrt{w})\right]$$
$$+ (1 - K_{atm}).\exp[-\sqrt{d}(\alpha_2 + \beta_2\sqrt{w}) \qquad (1)$$

$$w(w\%, T_{atm}) = w\%.\exp(h_1 + h_2.T_{atm} + h_3.T^2_{atm} + h_4.T^3_{atm}) \qquad (2)$$

where, $\omega$ is the coefficient indicating the content of water vapor in the atmosphere, w% is relative humidity, d is distance, $K_{atm}$ is the scaling factor for the atmosphere damping ($K_{atm}$ = 1.9), $\alpha_1$ and $\alpha_2$ are attenuation factors for atmosphere without water vapour, $\beta_1$ and $\beta_2$ are attenuation factors for water vapour, and $h_1$ = 1.5587, $h_2$=6.939 × 10$^{-2}$, $h_3$=−2.7816 × 10$^{-4}$, and $h_4$ = −6.8455 × 10$^{-7}$. With the environmental conditions during the tests and a relatively short distance between the IR camera and the targets, the atmospheric transmission ($\tau$) was almost equal to 1 in each test.

The reflected apparent temperature and emissivity (ranges from 0 to 1) were determined with the IR camera. It is to be noted that the emissivity of a material surface changes at different wavelengths, depending on the temperature of object, conditions of surface, and the inclination between IR camera and surface. Reflected apparent temperature is regarded as the apparent temperature of surrounding objects which was determined based on the method suggested by ASTM E1862 [70]. Since the orientation of each wall and its surrounding environment is different, the reflected apparent temperature was measured for each wall separately. To estimate the emissivity, a sample of 3 M Scotch Super 88 Vinyl black electrical tape with a known emissivity value equal to 0.95±0.02 was used following ASTM E1933 procedures [71]. It is to be noted that the emissivity of material is nearly independent of the ambient and material temperatures expected during building inspections. Furthermore, according to the Ref [72], the emissivity of materials remains constant in the range of 0 °C to 48 °C. To ensure accuracy, several measurements were performed, and the emissivity was estimated using the average of values.

Window glass is opaque in the long-wave IR range (4-14$\mu m$) and the insulated glass unit (IGU) has relatively lower thermal mass than the opaque building materials [73]. Consequently, the time for windows to achieve quasi stead-state conditions is significantly shorter than the opaque components. However, glass emissivity is lower than most opaque building materials, which ranges from 076 to 0.87 depending on the type of window materials and accuracy of sensors and the camera [73]. Also, since glass has specular reflections, emissivity measurement by IRT surveys are more influenced by surrounding radiation than opaque elements [73]. Furthermore, the reflection of the IR camera and thermographer as well as the incident angle can influence the accuracy of measurements. In this study, the W2 window was selected to determine the emissivity of glass since it was less exposed to the surrounding environment than other windows, namely adjacent buildings and parking lights. Ref [73–74] suggested that both reflectance and emissivity of glass remain almost constant for an incident angle under 45°. Therefore, to measure the emissivity of glass, the IR camera was positioned at the distance of 2 m from the outer surface of glass and thermal images were taken at different angles, including in front of the glass as well to either side of the glass within 45°. For each direction, the emissivity and reflected temperature was measured according to ASTM E1862 and ASTM E1933, respectively. The mean of measured values (0.85) was obtained as emissivity of the window.

Finally, to eliminate the impact of systematic error on U-value estimation, it is suggested to acquire as much data as possible with the same instrument [29,75]. Hence, apart from emissivity, reflected temperature and surface temperature, outdoor air temperature was also measured with the IR camera. In other words, the large uncertainty (±5°C) of the IR camera compared to the thermistors (±0.01 °C), as well as differences in their methods of measurement (non-contact & 2D temperature measurement vs. contact & point measurement), would result in different outdoor air temperature measurements and subsequent error in estimation of U-value [59]. To this end, a piece of cardboard (10 cm× 10 cm) with an emissivity of 0.95 was positioned near the wall exterior surface 2–3 h before the tests to ensure it reached thermal equilib-

rium with the environment. Since outdoor environmental conditions vary over time, the measurement was performed when the variations were minor prior to the tests (~3–4 h) and were relatively consistent at the time of survey. Consequently, outdoor air temperature was estimated by measuring the surface temperature of cardboard using instantaneous IRT [59].

Besides the impacts of the above-mentioned parameters on surface temperature measurements with IR cameras, uncertainties associated with the IR camera detector (composed of an uncooled microbolometer) were also considered in the analysis. The gain and offset of pixels in the detector are not identical due to camera temperature instability and ambient condition variability during the thermographic survey, as well as errors associated with manufacturing [59]. In general terms, the microbolometers also receive radiation from the camera's interior, which can be considerably higher than radiation from the objects, ultimately resulting in severe non-uniformity artefacts (a low-quality image). To improve the accuracy and reduce non-uniformity, the camera takes an image with the shutter closed and measures the IR radiation from its own optics [76]. The temperature of the shutter acts as a reference value for correcting images and is assumed to have a similar temperature with other IR camera components such as lens and optics [76]. This process is called Non-Uniformity Correction (NUC) and ensures a harmonized response signal across the sensors. NUC functionality can be performed automatically by the camera itself or manually by a thermographer. It is worth noting that these non-uniformities are present more often when the camera is first powered up and attempting to achieve temperature stability. Therefore, it is recommended to avoid thermography for the initial ~ 30 min to allow the camera to warm up in a stable environment to obtain the best temperature measurement accuracy [77]. To reduce uncertainties in this study, all surveys were started after a 30-minute camera warm-up period and NUC was performed manually before recording thermal images.

### 2.8. Overall effective U-value measurement with IRT

The overall thermal transmittance of wall assemblies was estimated by assuming that the heat flux is passing through the elements, and transferred to the IR camera sensors through radiation $q_r$ (W/m²) and convection $q_c$. Accurate calculation of radiation heat flux necessitates considering the view factor of all surrounding objects and their temperatures in the field of view of the wall assembly being studied as shown in Equation (3) [78].

$$q_r = \varepsilon\sigma[F_{sky}\left(T_{s,avg}{}^4 - T_{sky}{}^4\right) + F_{ground}\left(T_{s,avg}{}^4 - T_{ground}{}^4\right)$$
$$+ F_{air}\left(T_{s,avg}{}^4 - T_{air}{}^4\right) + F_{object-1}\left(T_{s,avg}{}^4 - T_{object-1}{}^4\right)$$
$$+ F_{object-2}\left(T_{s,avg}{}^4 - T_{object-2}{}^4\right) + \cdots \tag{3}$$

where $F_{sky}$ is the view factor of the sky, $F_{ground}$ is the view factor of the ground, $F_{air}$ is the view factor of the ambient air, $F_{object}$ is the view factor of surrounding objects, $T_{sky}$ is the temperature of the sky (defined as the temperature that the sky exchanges heat via radiation as a black body), $T_{ground}$ is the temperature of the ground, $T_{air}$ is the temperature of ambient air, and $T_{object}$ is the surface temperature of surrounding objects. The sum of all view factors is equal to 1.

$$\sum F_{sky} + F_{ground} + F_{air} + F_{objects} = 1 \tag{4}$$

Since experiments in this study were performed on overcast skies and ambient air temperature was stable several hours prior

to the tests, it was approximated that temperatures of the sky [29], the ground [79] and surrounding objects are in thermal equilibrium with ambient air. Therefore, radiation heat exchange of surfaces was assumed to be with the ambient air and view factor is equal to 1 [59].

In this study, the instantaneous U-value (W/(m² K)) was calculated using Equation (5):

$$U_{overall} = \frac{q_r + q_c}{T_{in} - T_{out}} = \frac{\varepsilon\sigma\left(T_{s,avg}{}^4 - T_{out}{}^4\right) + h_c(T_s - T_{out})}{T_{in} - T_{out}} \tag{5}$$

where $T_{s,avg}$ is the average of surface temperature of the opaque wall including thermal bridging (parapet, corners, and window frame), $T_{in}$ is the indoor air temperature (°C), $T_{out}$ is the outdoor air temperature in the vicinity of the target (°C), $\varepsilon$ is emissivity of wall, $\sigma$ Stefan-Boltzmann constant ($5.67\times10^{-8}$), and $h_c$ is the convective heat transfer coefficient (W/m² K).

The surface temperature of the opaque wall was measured using combinations of different-sized ROIs to exclude window and doors from analysis. Thermal images in Fig. 4 depicted the areas of thermal bridging and sources of air leakage in the wall assemblies. The average of surface temperature of ROIs was then determined based on an area-weighted approach:

$$T_{s,avg} = \frac{T_1 * A_1 + T_2 * A_2 + T_3 * A_3 + \cdots + T_i * A_i}{A_T} \tag{6}$$

where $T_{s,avg}$ is the average surface temperature of opaque areas, $A_i$ is the area of ROI, $T_i$ is the average of surface temperature corresponding to area $A_i$, and $A_T$ is the collective area of all ROIs.

The convective heat transfer coefficient $h_c$ was calculated based on the dimensionless method, which is a function of flow regimes, target geometry characteristics and air properties, calculated as shown in Equation (7).

$$h_c = \frac{Nuk}{L} \tag{7}$$

where $Nu$ is the Nusselt number [dimensionless], $L$ is the height of the wall (m) measured from the exterior, and $k$ is the thermal conductivity of the fluid (air). For air at 5–10 °C, $k$ is 0.024 W/m K.

For laminar flow over a wall surface, $Nu$ is determined by using the following equation:

$$Nu = 0.664Re^{1/2}Pr^{1/3} Pr > 0.6 \tag{8}$$

where ($Re$) and ($Pr$) are dimensionless Reynolds and Prandtl numbers. For air at 5–10 °C, $Pr$ = 0.71 was used [59].

### 2.9. Infrared index

The Infrared Index (IRI) was obtained based on the approximation of a steady-state condition where the rate of heat flux from the interior to the exterior is equal to the heat flux from the exterior surface to the outdoor air (assuming one-dimensional heat transfer). IRI is expressed as:

$$IRI = \frac{T_{s,avg} - T_{out}}{T_{in} - T_{out}} \tag{9}$$

where $T_{in}$ and $T_{out}$ are indoor and outdoor air temperatures, and $T_{s,avg}$ is average surface temperature of whole vertical building envelope measured by external IRT. As shown in Equation (6), measured $T_{s,avg}$ is comprised of thermal effects from the opaque wall
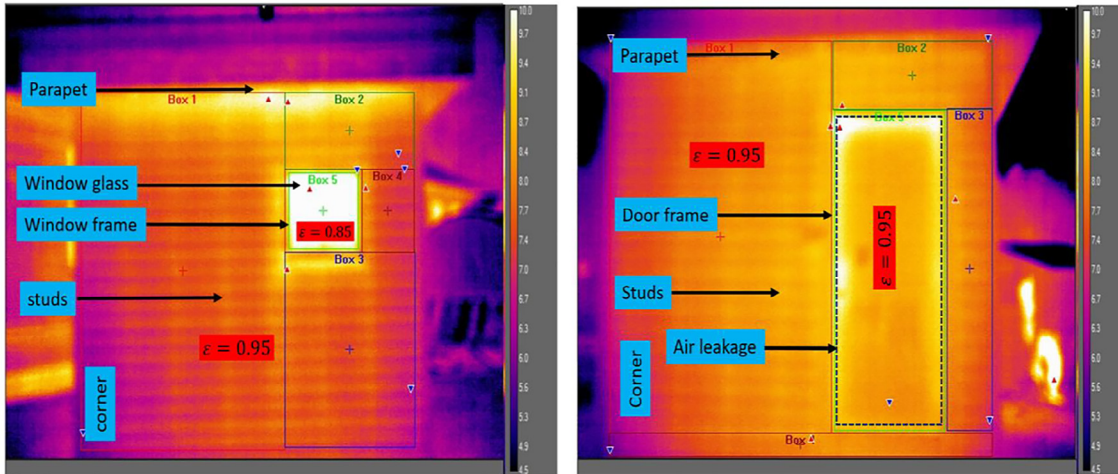
(a)                                                        (b)

**Fig. 4.** Thermal images of (a) W2, (b) W1. Example ROIs are denoted "Boxes"
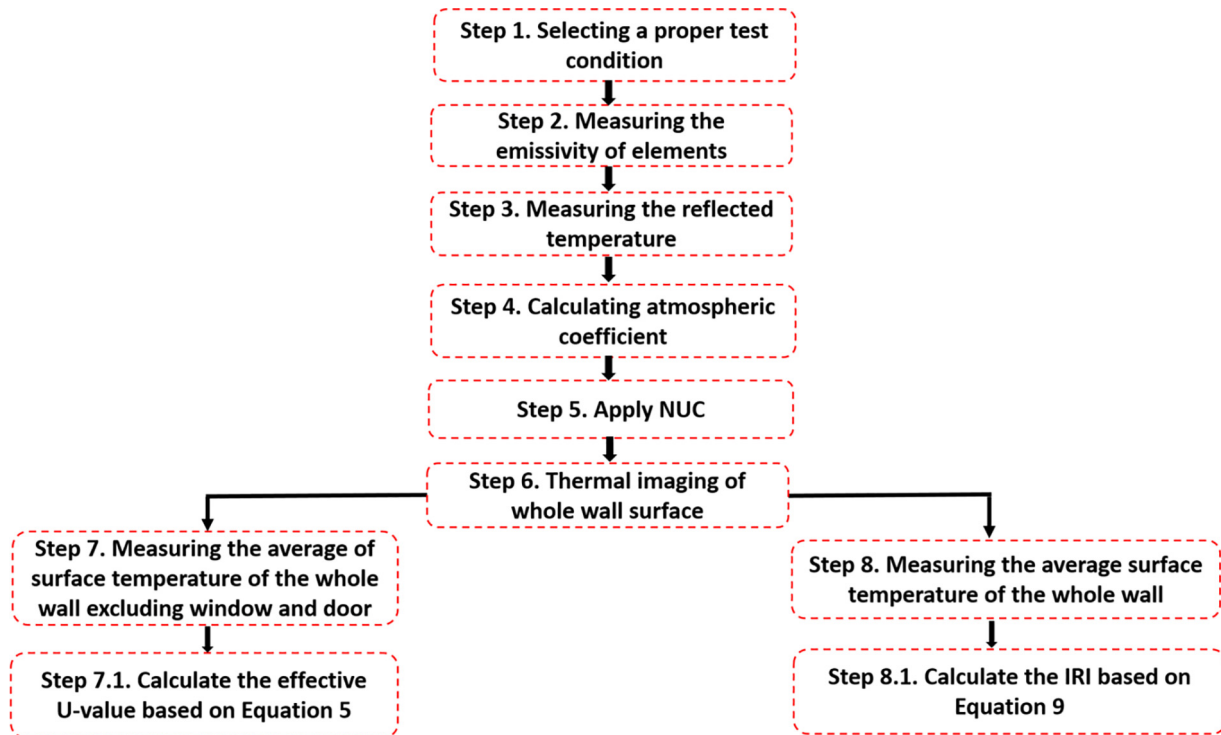


**Fig. 5.** External IRT measurement procedure to determine U-value and IRI.

including thermal bridging, fenestration (windows & doors), air leakage, and any other imperfections in the wall assembly.

A flowchart describing the procedure to calculate U-value and IRI is illustrated in Fig. 5.

### 2.10. Measurement uncertainty analysis on U-values and IRI

The U-value depends on several parameters, which was shown in Equation (5). The law of propagation of uncertainties was applied to determine the combined standard uncertainty of U-value based on all the measured parameters [64]. The uncertainty ($\Delta U$) was then obtained using the following expression:

$$\Delta U^2 = \sum_{i=1}^{n} \left(\frac{\partial U}{\partial X_i}\right)^2 \Delta X_i^2 \tag{10}$$

$$\Delta U^2 = \left(\frac{\partial U}{\partial T_{in}}\right)^2 .(\Delta T_{in})^2 + \left(\frac{\partial U}{\partial T_{out}}\right)^2 .(\Delta T_{out})^2 + \left(\frac{\partial U}{\partial T_s}\right)^2 .(\Delta T_s)^2$$
$$+ \left(\frac{\partial U}{\partial \varepsilon}\right)^2 .(\Delta \varepsilon)^2 + \left(\frac{\partial U}{\partial h}\right)^2 .(\Delta h)^2 \tag{11}$$

where $\Delta T_{in}$ is the uncertainty associated with indoor air temperature measuring equipment, $\Delta T_s$, $\Delta T_{out}$ and $\Delta \varepsilon$ are the uncertainties associated with infrared camera, and $\Delta h$ is the uncertainty in wind speed measured by the anemometer. The standard uncertainty of

each variable ($\Delta X_i$) was measured based on Type B uncertainty since no statistical treatment or repeated measurements analysis was performed. In other words, the data was not collected from a series of measurements, instead taken from manufactures' specifications. Furthermore, to convert manufacturer reported figures to standard uncertainty, a rectangular probability distribution of possible values was considered for all parameters, implying that all outcomes have an identical chance to occur.

The uncertainties of all variables were considered based on the half-width of the uncertainty limit as shown in Table 3. The standard uncertainty of emissivity obtained was 0.02, similar to the black tape uncertainty that was used during measurements. The sensitivity coefficients ($\frac{\partial U}{\partial X_i}$) of U-value are presented in Table 4, where by multiplying the sensitivity of each variable by its standard uncertainty ($\frac{\partial U}{\partial X_i}.\Delta X_i$), the uncertainty contribution of each variable on the output (U-value) can be obtained.

Similar to U-value, sensitivity coefficients for IRI are shown in Table 5.

### 2.11. Calculation of effective thermal transmittance (U-value)

The effective thermal transmittance (U-value) of walls were determined using Equation (12). To summarize this approach, the overall thermal transmittance comprised of three components:

(1) **Clear field transmittance** ($U_o$) is the heat flow from the wall assembly including the effects of uniformly distributed thermal bridging components, such as structural framing (studs), and structural cladding attachments.
(2) **Linear transmittance** ($\Psi$).is the additional heat flow caused by linear thermal bridging details including slab edges, corners, parapets, and transitions between assemblies.
(3) **Point transmittance** ($\chi$) is the heat flow caused by thermal bridging details that occur only at a single or infrequent locations including building components such as structural beam penetrations and intersections between linear details.

$$U_{effective} = \frac{\sum(\Psi \cdot L) + \sum(\chi)}{A_{total}} + U_o \qquad (12)$$

where $U_{Total}$ is total effective assembly thermal transmittance (W/m²K), $U_o$ is the clear field thermal transmittance (W/m²K) which calculated from from 3D simulation values [42,80], $A_{total}$ is the total opaque wall area (m²), $\Psi$ is heat flow from linear a thermal bridge (W/m K) obtained from 3D simulation details in the BETB [42], L is the length of a linear thermal bridging detail as shown in Table 6, and $\chi$ is a point source thermal transmittance (W/K). It should be noted that since the structure was constructed on pier blocks instead of a typical foundation slab, thermal bridging to the ground is negligible. Likewise, due to a lack of structural penetrations point source thermal bridges are effectively absent. Hence, the remaining thermal bridging recorded in the measurements are a result of the wall-roof interface (parapet), corners, window/door-wall interfaces, studs, and cladding structural attachment systems (girts). The overall thermal transmittance of wall assemblies in this study is shown in Table 7.

**Table 3**
Uncertainties of equipment used for U-value measurements.

| Parameters | Sensors | Uncertainty half-width limit $\pm$ |
|---|---|---|
| Wall surface temperature | IR camera | 5 °C |
| Outdoor air temperature | IR camera | 5 °C |
| Indoor air temperature | Temperature sensor | 0.01 °C |
| Wind velocity | Anemometer | 0.1 m/s |

**Table 4**
Sensitivity coefficients for the implementation of the law of error propagation in U-value estimation by using outdoor infrared thermography.

| Variable $X_i$ | Sensitivity coefficient $\frac{\partial U}{\partial X_i}$ |
|---|---|
| $T_s$ | $\frac{h + 4.\varepsilon.\sigma.T_s^3}{T_{in} - T_{out}}$ |
| $T_{in}$ | $-\frac{\varepsilon.\sigma.(T_s^4 - T_{out}^4) + h_c.(T_s - T_{out})}{(T_{in} - T_{out})^2}$ |
| $T_{out}$ | $-\frac{(4.\varepsilon.\sigma.T_{out}^3 + h).(T_{in} - T_{out}) + [h_c.(T_s - T_{out}) + \varepsilon\sigma(T_s^4 - T_{out}^4)]}{(T_{in} - T_{out})^2}$ |
| $\varepsilon$ | $\frac{\sigma(T_s^4 - T_{out}^4)}{T_{in} - T_{out}}$ |
| $h_c$ | $\frac{T_s - T_{out}}{T_{in} - T_{out}}$ |

**Table 5**
Sensitivity coefficients for IRI estimation with external IRT.

| Variable $X_i$ | Sensitivity coefficient $\frac{\partial IRI}{\partial X_i}$ |
|---|---|
| $T_s$ | $\frac{1}{T_{in} - T_{out}}$ |
| $T_{in}$ | $-\frac{T_s - T_{out}}{(T_{in} - T_{out})^2}$ |
| $T_{out}$ | $\frac{T_s - T_{in}}{(T_{in} - T_{out})^2}$ |

**Table 6**
Summary of linear thermal bridges.

| Thermal Bridge Type | Ψ-value (W/m K) | Length (m) | Heat Flow (W/K) |
|---|---|---|---|
| wall-roof interface (interior insulated walls) | 0.05 | 3.05 | 0.09 |
| wall-roof interface (exterior insulated walls) | 0.08 | 3.05 | 0.15 |
| window/door-wall interface (interior insulated walls) | 0.001 | 1.6 | 0.38 |
| window-wall interface (exterior insulated walls) | 0.035 | 1.6 | 0.14 |
| Corner | 0.04 | 6.10 | 0.24 |

**Table 7**
U-values of walls.

| Wall Assembly | Nominal U-value (W/m² K) | Clear field $U_0$-value (W/m² K) | Effective U-value (W/m² K) |
|---|---|---|---|
| W1 | 0.34 | 0.37 | 0.43 |
| W2 | 0.23 | 0.26 | 0.31 |
| W3 | 0.16 | 0.20 | 0.26 |
| W4 | 0.16 | 0.18 | 0.24 |

### 2.12. Dynamic energy model

An energy model was developed using EnergyPlus, which included inputs for U-value (walls, roof, window, door, floor), internal loads (a laptop), air leakage rate, and electric resistance heating. Building geometry was developed in SketchUp, integrated with an OpenStudio plug-in that translates information to EnergyPlus syntax.

To assess sensitivity of IRT measurements on the energy model, three model scenarios were considered with different building envelope inputs:

- 1D U-values (without considering the impact of thermal bridging and attachment components) inferred from IRT measurements
- 2D effective U-values inferred by IRT
- 2D effective U-values inferred by IRT with vignetting artefact correction

Simulation outputs were compared against metered energy consumption. The energy modelling framework is illustrated in Fig. 6.

Accuracy of energy models were examined based on two statistical uncertainty indices (1) Normalized Mean Bias Error (NMBE), and (2) the Coefficient of Variation of the Root Mean Square Error (CVRMSE). These indices are defined by ASHRAE Guideline 14–2014 [81] for the calibration of energy models. Equation 13 shows the calculation of NMBE where $m_i$ is the measured value, $s_i$ is the simulated data, $n$ is the number of measured data points, and $p$ is the number of adjustable model parameters, which for calibration is suggested to be 0.

$$\text{NMBE} = \frac{1}{\bar{m}} \cdot \frac{\sum_{i=1}^{n}(m_i - s_i)}{n-p} \times 100 (\%) \quad (13)$$

CV(RMSE) is obtained based on Equation 14, where the value of $p$ is suggested to be 1.

$$\text{CV(RMSE)} = \frac{1}{\bar{m}} \sqrt{\frac{\sum_{i=1}^{n}(m_i - s_i)^2}{n-p}} \times 100 (\%) \quad (14)$$

The model is then considered calibrated if NMBE and CVRMSE are less than $\pm 5\%$ and 15%, respectively [40].

## 3. Results & discussion

### 3.1. Determination of U-value

The effective U-value (i.e. 2D U-value) obtained from the 2D thermogram for the entire wall system was estimated for Day 1 to Day 3. Figs. 7 and 8 show the surface temperature distribution in W1 and W2, illustrating non-uniformity distribution around thermal bridging such as wood framing, the window frame, the parapet, and likely due to air leakage at the wall-to-door interface in W1. ROIs were selected to cover the opaque wall (excluding fenestration). W3 and W4 are not presented for brevity, since thermal patterns are similar to that of W2. The "Fusion Palette" colour rendering scheme was chosen to represent surface temperature where bright yellow corresponds to warmer pixels and dark blue represents colder pixels. For instance, pixel intensity around the parapet and window frame were higher most likely as a result of thermal bridging. In contrast, pixel intensity at the corners of the structure appear colder than in the centre which is an artefact of a profound vignetting effect, but could also be confounded by thermal bridging to some extent. It is worth mentioning that although the wall-to-roof interface does not have a large psi-value, temperature gradients inside the structure due to stack effect (temperature around the ceiling is higher) led to a higher conductive heat loss (higher pixel intensity in thermal images) around that area. Thermocouple measurements confirm temperature gradients of ~1 °C between the lowest and highest reading heights. It is unknown to what extent air leakage could also contribute to this finding.

The results in Table 8 show U-values were not identical on different days, even though tests were performed under relatively steady-state conditions. This implies that in practice, steady-state conditions are never achieved, unlike calculated values which are obtained under steady-state conditions. In other words, calculated U-values obtained using 3D simulation tools ignore the impact of surrounding objects' radiation (both emission and reflection) and fluctuations of the outdoor condition such as temperature, relative humidity and wind before and during the tests. Hence, U-value of a wall changes based on its location, orientation of buildings, the construction type (i.e., wood vs. concrete), number of surrounding buildings, and the variation of environmental conditions (wind, temperature, humidity). For instance, W1 & W3 were in the field of view of the adjacent conditioned lab building where the exchange of radiation between surfaces was present at the time of tests even though the lab building was wood-framed building (low thermal mass) and tests were performed in late night (ensuring a relatively steady-state condition). Higher reflected temperature in W1 & W3 (~1.5 °C) compared to the W2 & W4 confirmed this fact. It should be remarked that U-values by IRT were obtained based on 2D thermal images and their deviations with 3D simulation values are undeniable and should be considered in practice.

Additionally, interior insulated walls (W1 & W2) had relatively lower deviations compared to those with split-insulated assemblies (W3 & W4), confirming the findings of Albatici et al. [29] and Dall'O' et al. [28] that IRT is less accurate for well-insulated walls: a lower thermal heat flux implies a small difference between
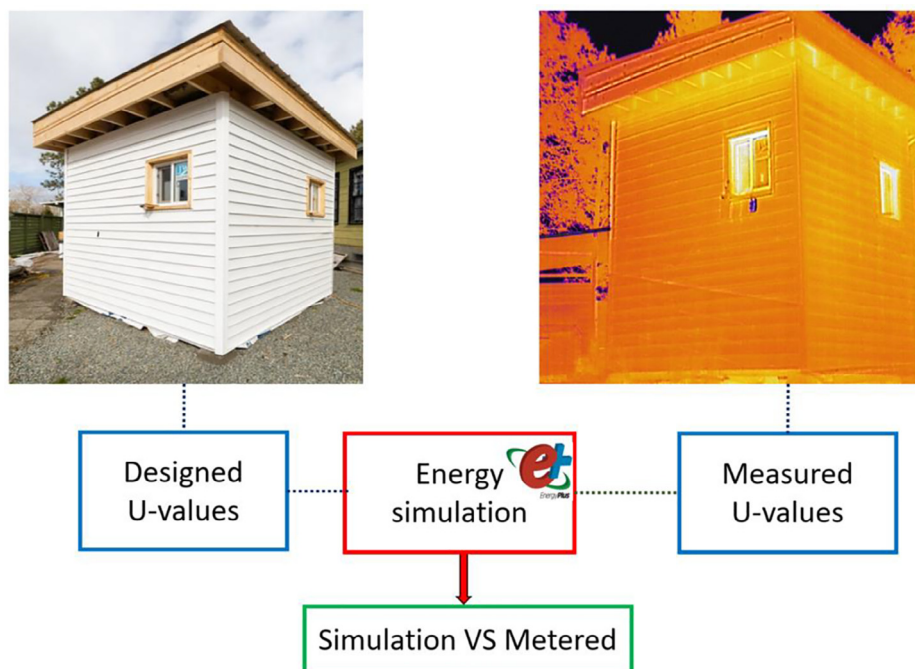


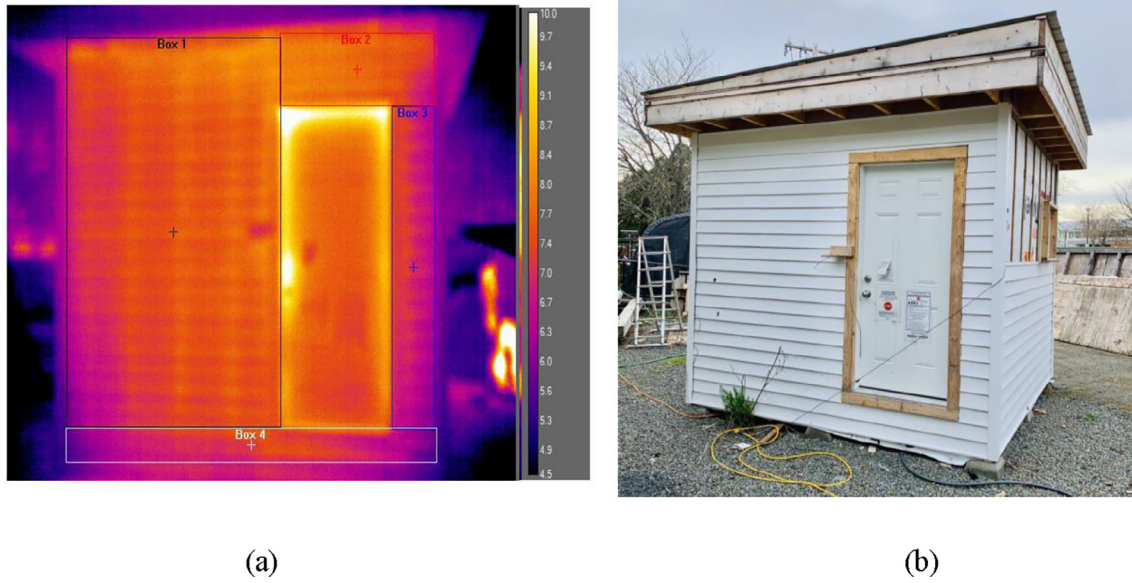**Fig. 6.** Development of a building energy model based different approaches.

(a)

(b)

**Fig. 7.** Selection of region of interests (ROIs) to estimate U-value of W2: (a) thermal image; and (b) photograph.



(a)

(b)

**Fig. 8.** Selection of region of interests (ROIs) to estimate U-value of W1: (a) thermal image; and (b) photograph.

**Table 8**
Comparison of IRT-estimated and simulated U-values on different days.

| Wall assemblies | IRT-estimated 2D U-value (W/m² K) | 3D simulated U-value (W/m² K) | Deviations (%) |
|---|---|---|---|
| Day 1 | | | |
| W1 | 0.37 | 0.43 | −13.95 |
| W2 | 0.22 | 0.31 | −29.03 |
| W3 | 0.09 | 0.26 | −65.38 |
| W4 | 0.04 | 0.24 | −83.33 |
| Day 2 | | | |
| W1 | 0.35 | 0.43 | −18.60 |
| W2 | 0.26 | 0.31 | −16.13 |
| W3 | 0.11 | 0.26 | −57.69 |
| W4 | 0.06 | 0.24 | −75.00 |
| Day 3 | | | |
| W1 | 0.37 | 0.43 | −13.95 |
| W2 | 0.25 | 0.31 | −19.35 |
| W3 | 0.15 | 0.26 | −42.31 |
| W4 | 0.10 | 0.24 | −58.33 |

the exterior wall surface (exterior insulation) and the surrounding outdoor air, allowing environmental and climatic variability to impact exterior surface temperatures to a more significant extent. This trend was repeated on all days; however, results on Day 3 were slightly better for W3 and W4, which can be attributed to a lower wind speed. It is worth pointing out that U-value estimations were based on cladding surface temperatures which may not represent the actual surface temperature of exterior surface due to the 19 mm gap between cladding and wall exterior surface. However, as mentioned in Ref [59], assuming the cladding has a relatively similar temperature to the exterior surface is justifiable due to low wind speed at the time of the tests, resulting in limited air flow and little convection heat exchange in the cavity (radiation heat exchange between surfaces was dominant).

To understand if the lower pixel intensity around corners was a result of vignetting or thermal bridging, other images were taken from different incident angles. Fig. 9 illustrates histograms of ROIs
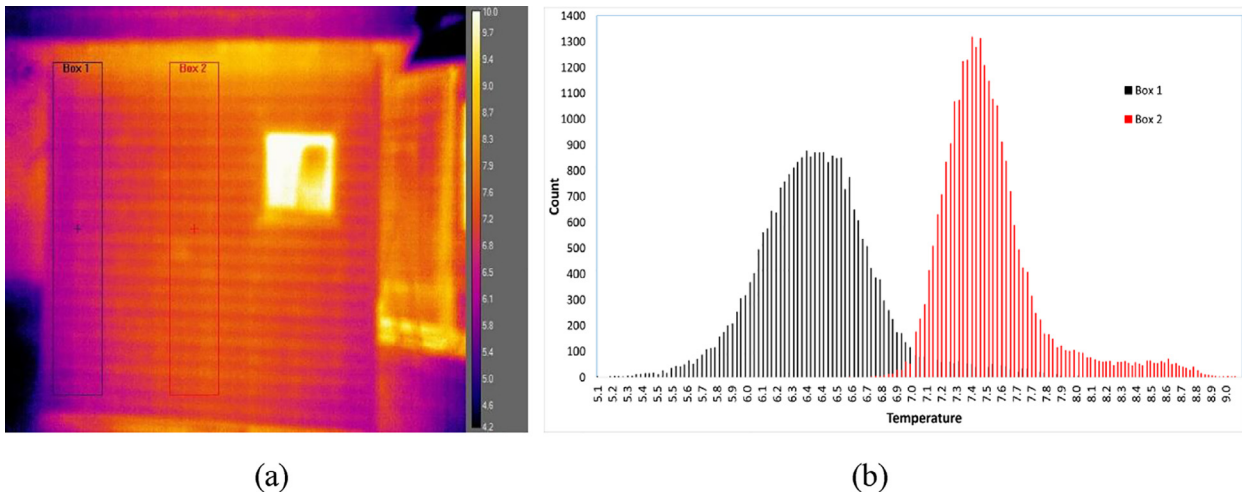
(a)                                                                                    (b)

**Fig. 9.** Evaluation of corners based on (a) two selected ROIs (Boxes 1 & 2) thermal images; and (b) temperature distribution histograms.

selected to form a baseline comparison, confirming that temperatures in Box 1 (near the corner) were lower than Box 2 (centre of wall) by ~ 1 °C and had a wider distribution (greater standard deviation). However, thermal images taken from a different angle with the same corner in the centre (Fig. 10) showed temperature data similar to that of Box 2 in Fig. 9. It can be deduced that the vignetting effect is dominant around the corners of a thermogram and should be accounted for to improve accuracy. Hence, it was decided to divide the wall into six segments (Fig. 11). The thermal image for each segment was taken separately to ensure that the segment was in the centre of thermal images, limiting the effect of vignetting. Finally, segments were stitched together to form a new thermal image with corrected values as shown in Fig. 12. U-values for all walls were re-calculated yielding substantial improvements in accuracy, ranging from −2.33% to −12.50% (Table 9) versus −13.95% to −58.33% using the single-thermogram methodology (Table 8). It should be noted that vignetting effect intensified surface temperature reduction in W3 & W4 (surface temperature was closer to outdoor air compared to W1 & W2), particularly around the corners where temperatures were below the outdoor air temperature (negative U-value), unlike W1

& W2. Therefore, improvement in accuracy of U-values in W3 & W4 was considerably larger than those in W1 & W2, suggesting that vignetting effect could have a more adverse impact in well-insulated wall assemblies.

### 3.2. Infrared index (Relative quantitative comparison)

Results in Section 4.1 showed that due to the instability of outdoor conditions, U-values estimated with IRT may differ on different days, even if the tests are each performed in approximately steady-state conditions. To validate IRI as a ranking metric for building envelope thermal performance, index values were calculated on five different days with varying external conditions; IRI rankings were then compared with their overall U-values. Notably, the calculation of overall building envelope U-values also included the door and windows. Ranking based on simulated U-values demonstrated that W4 had the best thermal performance, followed by W3, W2 and W1. Simulated values only consider heat loss through the clear field areas and the effect of thermal bridging, while the impact of air leakage or any other defects was ignored in this ranking (Fig. 13). Since W2, W3 and W4 have windows
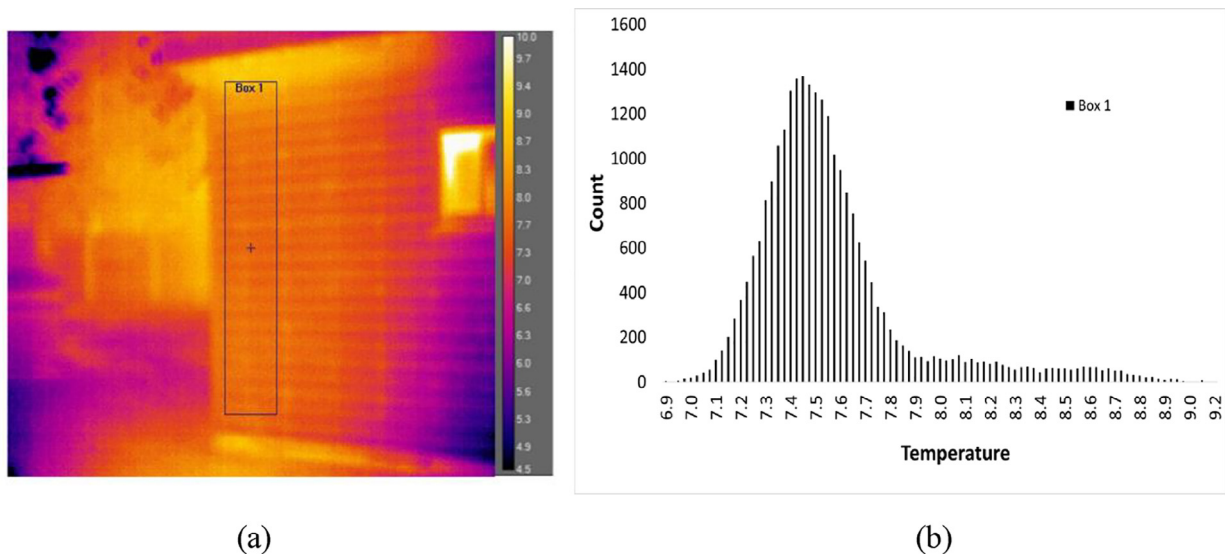


(a)                                                                                    (b)

**Fig. 10.** Evaluation of temperature distribution of Box 1 from a different angle: (a) Box 1 located in the centre of the image; and (b) temperature distribution histograms.
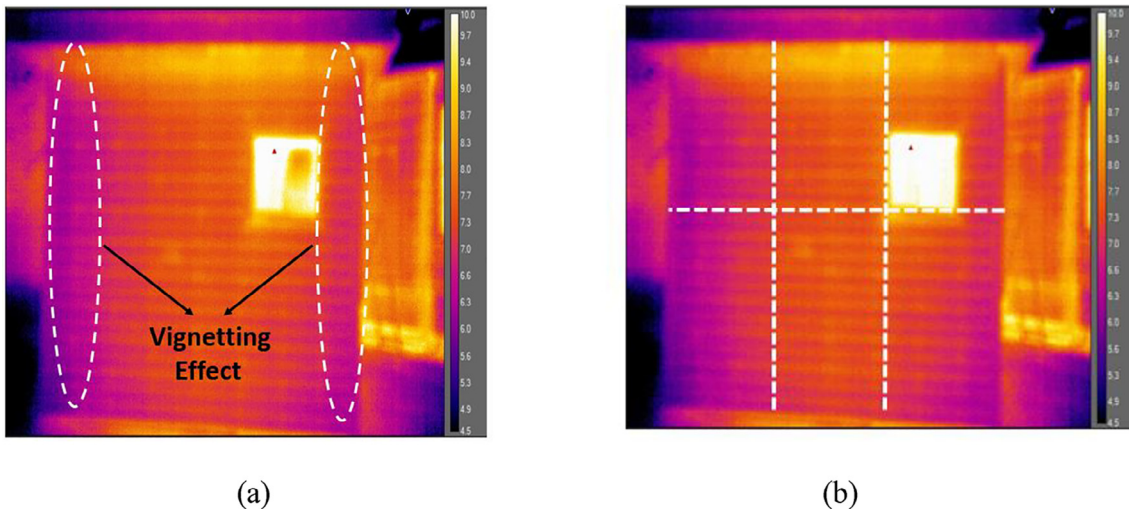
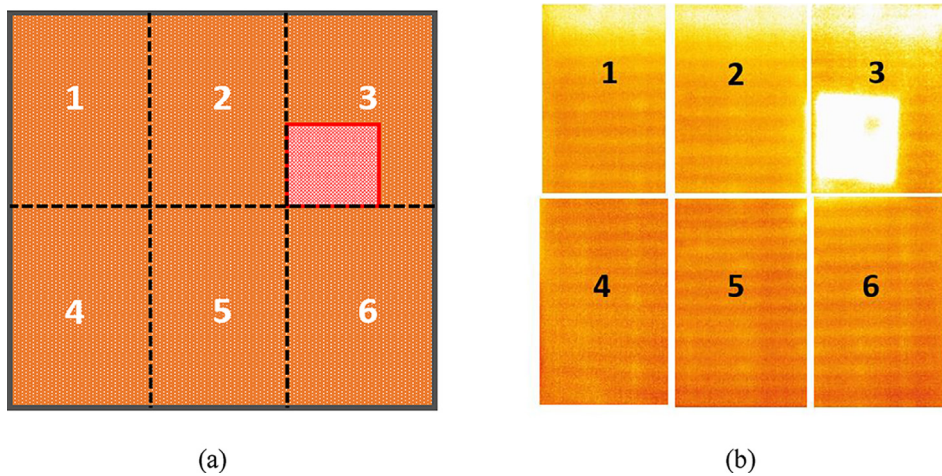**Fig. 11.** (a) identification of vignetting effect; (b) Dividing the thermal image into six segments.



**Fig. 12.** (a) Schematic segments of thermal images; (b) Combined thermal images from different angle.

**Table 9**
Comparison of IRT-estimated and simulated U-values on Day 3 after accounting for the vignetting effect.

| Wall assemblies | IRT-estimated 2D U-value (W/m² K) | 3D simulated U-value (W/m² K) | Deviation (%) |
|---|---|---|---|
| W1 | 0.42 | 0.43 | −2.33 |
| W2 | 0.29 | 0.31 | −6.45 |
| W3 | 0.23 | 0.26 | −11.53 |
| W4 | 0.21 | 0.24 | −12.50 |

(similar sources of thermal bridging), only W2 is presented in Fig. 13 for brevity. In IRI calculations, surface temperature of the entire wall (including windows and door) were considered. Fig. 14 depicts IRI for each wall measured on different days and shows a similar ranking in spite of variations in external conditions. Furthermore, IRI ranking was identical to U-value ranking (Fig. 15). In other words, higher IRIs correlate to higher U-values. This implies that IRI can be appropriate for ranking and/or relative comparison of building envelope thermal performance. It should be noted that IRI considers the aggregated impact of building envelope effective thermal performance (opaque area) as well as air leakage, defects, and fenestration (Fig. 13). Hence, more thermal anomalies in the building envelope can lead to a higher IRI and a poorer overall thermal performance. This informs that higher levels of insulation do not necessarily ensure better building energy performance if air leakage, construction defects, and thermal bridging effects are substantial. In this sense, IRI can be more representative of the overall thermal performance of building envelope assemblies than IRT-estimated or 3D-simulated U-values. Perhaps most importantly, it provides the opportunity for quick surveys for a large number of buildings.

### 3.3. Uncertainty analysis

Uncertainties in U-value measurements with external IRT for each wall are shown in Tables 10 to 13, as a function of each input. Input values were taken from the test measurement on Day 3 after correcting the vignetting effect in thermal images. The reported values for surface temperature in Tables 10 to 13 were based on average surface temperature (Equation (6)). Since the variations of coefficients between the walls were too small, it was decided to report the U-values and uncertainties with three decimals in Table 10 to 13. The total standard uncertainty of measured U-values was 2–7 times larger than the calculated U-values suggesting significant uncertainty in U-value estimation with external IRT. This can be attributed to the high uncertainty of the IR camera
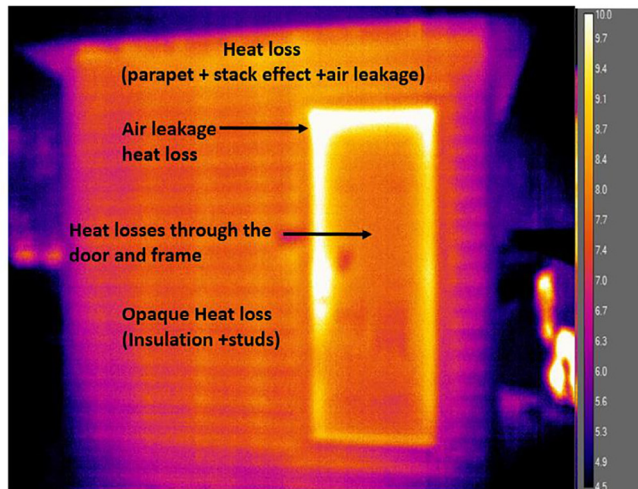
(a)
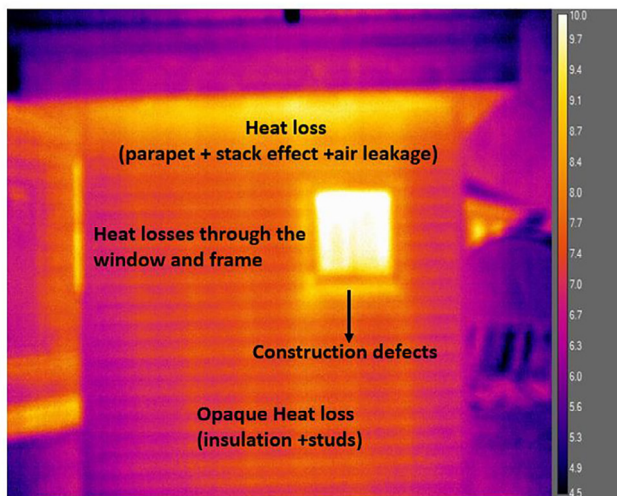


(b)

**Fig. 13.** Sources of heat losses through the building envelope: (a) W1; (b) W2.

(±5°C) used for surface and outdoor air temperature measurements. Hence, although obtaining as many data as possible with the same instrument improved accuracy of results, it had an adverse effect on uncertainty.

The sensitivity of the U-value to parameters for each wall is reported in the second column of Tables 10-13. Differences in wall thermal performance resulted in deviations in the sensitivity coefficient accordingly. It is seen that the sensitivity coefficient for surface temperature in W1 was larger than in other walls, but had the smallest sensitivity to outdoor air temperature. This confirms the significant impact of outdoor air temperature on U-values of well-insulated walls (W3 & W4) which is similar to the findings of Albatici et al. [29]. In general, it can be deduced that outdoor air temperature has a significant impact on external IRT of well-insulated wall assemblies. Interestingly, emissivity had the highest sensitivity coefficient in W1, while it was the third-highest coefficient for other walls. This was consistent with the findings of Fokaides et al. [26] and Madding [25] that indicated emissivity has a significant impact on surface temperature measurements, and consequently U-value. However, since variations in wind speed influence the convective heat transfer coefficient, it is seen that uncertainty in the calculation of convective heat transfer coef-

ficient resulted in higher uncertainty in W1, due to a larger difference between surface temperature and outdoor air temperature (larger variation in the convection heat transfer term in the U-value equation). Finally, all walls were least sensitive to indoor air temperature (smallest in the case of W4). This trend was consistent for IRI of each wall, which was most sensitive to surface temperature and outdoor air temperature and least sensitive to indoor air temperature (Table 14). This is important from a practical perspective since it supports the feasibility of non-invasive thermography, effectively not requiring access to the building interior or building automation system (BAS) data to obtain reasonable results [82].

High sensitivity of wall assemblies to variables does not ensure high uncertainty contribution since uncertainty contribution considers both sensitivity coefficient and standard uncertainty of variables. For instance, all walls were sensitive to emissivity (highest in the case of W1). However, emissivity, along with indoor air temperature and convective heat transfer coefficient, contributes considerably <1% to the total uncertainty of the walls analyzed. However, surface temperature and outdoor air temperature had the highest contribution to total U-value uncertainty since both were measured with the IR camera, which has large standard uncertainty compared to sensors. The index column shows these variables collectively account for almost 98% of the total standard U-value uncertainty budget. Finally, indoor air temperature had the least uncertainty contribution due to small uncertainty temperature sensor (very accurate) and sensitivity coefficient.

### 3.4. Energy simulation analysis

Building energy models were developed in EnergyPlus to study impacts of the IRT methodologies in more practical terms. Fig. 16 compares the energy use of the structure for three scenarios including simulations based on (1) 1D U-values inferred from IRT measurements, (2) 2D effective U-values inferred by IRT, and (3) 2D effective U-values inferred by IRT with vignetting artefact correction. Energy models were compared with monthly metered energy data to examine accuracy of simulations. Simulations used weather data corresponding to the time period of metered consumption data.

To quantify the effect of 1D U-value determination by IRT (Table 15) on energy model accuracy, a region of interest (ROI) was considered in the centre of thermal images as suggested by Ref [59] to avoid the vignetting effect (Fig. 17). The ROI was selected between framing (studs) to minimize any thermal bridging or lateral heat flux contributions to surface temperature, and consequently U-value. Table 16 summarizes deviations of −8.70 to 23.53% between estimated 1D U-value by IRT and nominal 1D U-values (obtained without considering thermal bridging effects of studs and attachment components). Fig. 16 illustrates that simulations based on estimated U-values underestimate energy consumption (positive CVRMSE & NMBE values); or in other words, overestimated the thermal performance of the wall. The error became more substantial when the models were based on 1D U-values or effective U-values with vignetting, evident also in Fig. 16. However, model error is significantly reduced after correcting for vignetting (increased the accuracy of U-value calculations): NMBE < 5% and CVRMSE < 15% were satisfied per ASHRAE Guideline 14 criteria. Interestingly, models based 1D U-value and effective U-values with vignetting were almost similar. In 1D U-value calculations, the effect of any thermal bridging was neglected, which resulted in lower temperatures and ultimately a lower U-value. It appears that the combined effect of including for thermal bridging effects and vignetting artefacts had an approximately net-zero effect on effective U-value, and therefore also on energy consumption. This may be strictly a coincidence with the current
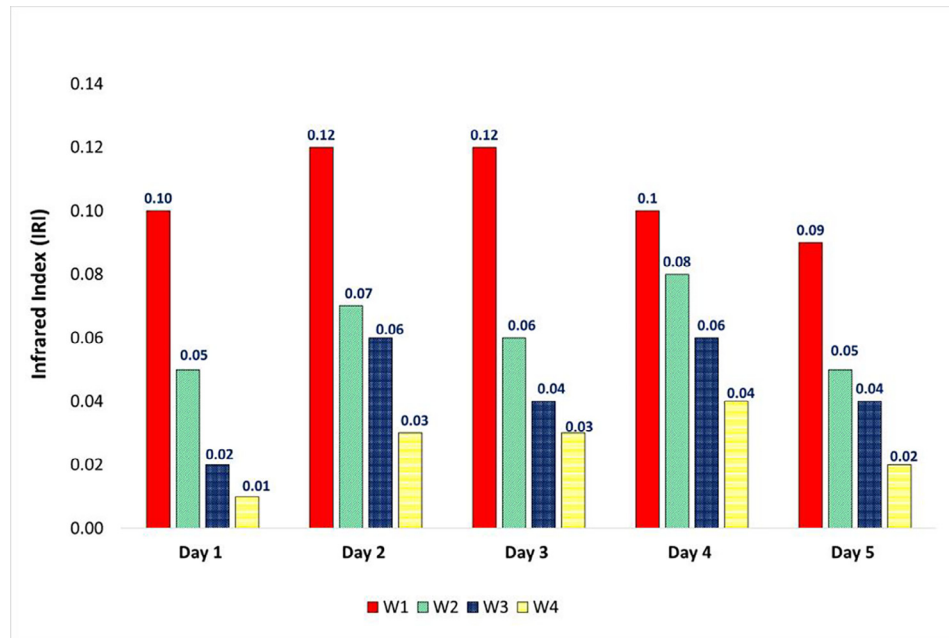
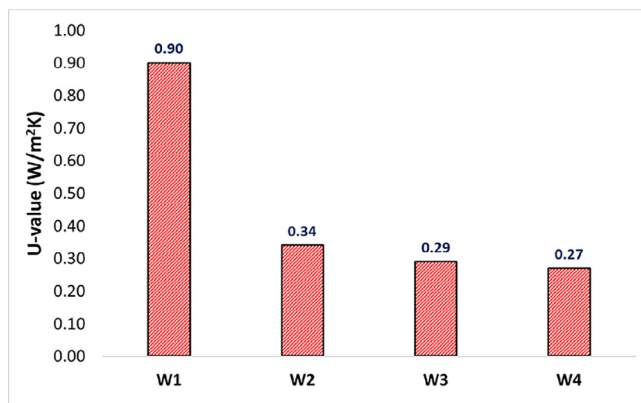**Fig. 14.** IRI of walls on different days.



**Fig. 15.** Wall rankings based on calculated U-values.

experimental set-up. Nonetheless, these findings suggest utilizing IRT to estimate U-value for use as inputs in an energy model should first (1) consider the effect of thermal bridging, and (2) address the adverse effect of vignetting.

In Section 4.1, it was shown that U-values calculated on different days can vary and impact energy model results. Hence, calibrating the energy model based on U-value calculated on a single day may not be representative. As with any model calibration, it is suggested that the climate data is from the nearest or otherwise most representative climate station and temporally corresponding to metered data. Energy model input U-values estimated using IRT should be obtained from the same time period.

## 4. Conclusions

This paper attempted to demonstrate the application of external IRT for quantitative analysis of building envelope thermal performance. The thermal characteristics of four different insulated wood-framed wall assemblies were estimated and compared with designed values obtained by 3D simulation tools. Also, the impact of vignetting artefact on the accuracy of results was examined, and a practical approach was developed to limit deviation of results with design values. Furthermore, impact of the accuracy of U-value estimated with IRT on the deviation of energy simulation outputs with metered data was examined. A comprehensive uncertainty analysis was conducted to determine the most influential parameters and their contribution to the uncertainty of results. Finally, a novel infrared index (IRI) was introduced as a metric for rapid evaluation and comparison of building envelope thermal performance.

The main findings of this study are highlighted as follows:

- Due to variation of outdoor environmental parameters, U-value estimates were not identical on different days.
- Vignetting has a substantial effect on the accuracy of results, particularly for well-insulated walls due to small differences between external surface and outdoor air temperatures.

**Table 10**
Uncertainty budget in U-value estimation with IRT for W1.

| Uncertainty Budget - W1 | | | | | |
|---|---|---|---|---|---|
| | Value | Sensitivity Coefficient | Standard Uncertainty | Uncertainty Contribution | Index (%) |
| Emissivity | 0.95 | 0.389 | 0.02 | 0.008 | 0.003 |
| Stephan- Boltzmann | $5.67 \times 10^{-8}$ | – | – | – | – |
| Wall temperature (K) | 281.35 | 0.355 | 2.886 | 1.025 | 54.71 |
| Outdoor air temperature (K) | 280.15 | −0.323 | 2.886 | −0.932 | 45.29 |
| Indoor air temperature (K) | 295.65 | −0.027 | 0.006 | −0.000 | 0.00 |
| Convection heat transfer coefficient (W/m² K) | 0.701 | 0.077 | 0.057 | 0.004 | 0.001 |
| U-value (W/m² K) | **0.419** | | | **1.385** | |

**Table 11**
Uncertainty budget of U-value measurement with IRT for W2.

| Uncertainty Budget- W2 | | | | | |
|---|---|---|---|---|---|
| | Value | Sensitivity Coefficient | Standard Uncertainty | Uncertainty Contribution | Index (%) |
| Emissivity | 0.95 | 0.268 | 0.02 | 0.005 | 0.001 |
| Stephan- Boltzmann | $5.67 \times 10^{-8}$ | – | – | – | – |
| Wall temperature (K) | 280.930 | 0.354 | 2.886 | 1.022 | 53.35 |
| Outdoor air temperature (K) | 280.150 | −0.331 | 2.886 | −0.955 | 46.65 |
| Indoor air temperature (K) | 295.650 | −0.019 | 0.006 | −0.000 | 0.00 |
| Convection heat transfer coefficient (W/m$^2$ K) | 0.701 | 0.054 | 0.057 | 0.003 | 0.0005 |
| U-value (W/m$^2$ K) | **0.289** | | | **1.398** | |

**Table 12**
Uncertainty budget of U-value measurement with IRT for W3.

| Uncertainty Budget- W3 | | | | | |
|---|---|---|---|---|---|
| | Value | Sensitivity Coefficient | Standard Uncertainty | Uncertainty Contribution | Index (%) |
| Emissivity | 0.95 | 0.219 | 0.02 | 0.004 | 0.001 |
| Stephan- Boltzmann | $5.67 \times 10^{-8}$ | – | – | – | – |
| Wall temperature (K) | 280.820 | 0.353 | 2.886 | 1.020 | 52.61 |
| Outdoor air temperature (K) | 280.150 | −0.335 | 2.886 | −0.978 | 47.38 |
| Indoor air temperature (K) | 295.650 | −0.015 | 0.006 | −0.000 | 0.00 |
| Convection heat transfer coefficient (W/m$^2$ K) | 0.701 | 0.043 | 0.057 | 0.002 | 0.0002 |
| U-value (W/m$^2$ K) | **0.233** | | | **1.404** | |

**Table 13**
Uncertainty budget of U-value measurement with IRT for W4.

| Uncertainty Budget- W4 | | | | | |
|---|---|---|---|---|---|
| | Value | Sensitivity Coefficient | Standard Uncertainty | Uncertainty contribution | Index (%) |
| Emissivity | 0.95 | 0.193 | 0.02 | 0.003 | 0.001 |
| Stephan- Boltzmann | $5.67 \times 10^{-8}$ | – | – | – | – |
| Wall temperature (K) | 280.750 | 0.352 | 2.886 | 1.017 | 52.17 |
| Outdoor air temperature (K) | 280.150 | −0.337 | 2.886 | −0.977 | 47.82 |
| Indoor air temperature (K) | 295.650 | −0.013 | 0.006 | −0.000 | 0.00 |
| Convection heat transfer coefficient (W/m$^2$ K) | 0.701 | 0.038 | 0.057 | 0.002 | 0.0001 |
| U-value (W/m$^2$ K) | **0.209** | | | **1.406** | |

**Table 14**
IRI sensitivity coefficients.

| Sensitivity Coefficient ($\frac{\partial IRI}{\partial X_i}$) | | | | |
|---|---|---|---|---|
| | W1 | W2 | W3 | W4 |
| Wall temperature (K) | 0.065 | 0.065 | 0.065 | 0.065 |
| Outdoor air temperature (K) | −0.058 | −0.061 | −0.063 | −0.064 |
| Indoor air temperature (K) | −0.006 | −0.003 | −0.002 | −0.001 |

- The proposed approach for addressing the vignetting effect resulted in substantial improvements in accuracy, ranging from −2.13% to −12.50% versus −13.95% to −58.33%.
- Although in-situ 2D U-value estimation of whole opaque wall assemblies using external IRT in this study has not been conducted previously, the findings of this investigation are in line with previous conducted quantitative IRT studies in a climate chamber from Tejedor et al. [11,62], which informed that the average 2D U-value estimation of facades by considering the effect of thermal anomalies facilitated a better and more accurate diagnosis of building envelope thermal performance.
- Wall thermal performance rankings based on infrared index (IRI) were consistent with their U-value rankings, implying that IRI can be a reliable metric for relative quantitative comparison of building envelope thermal performance, regardless of boundary conditions.

- Unlike effective U-value calculations that only considers heat loss through the clear field assemblies and the impact of thermal bridging in the building envelope, IRI considers all sources of heat losses including air leakage, thermal bridging and construction defects in building envelope. For the relatively new and carefully constructed at-scale structure used in this study, these other thermal anomalies are expected to be minor; however, for older buildings or poorly detailed building envelope assemblies, IRI may be a more holistic representation of relative thermal performance, although further research is needed to confirm the extent and to quantify the effects scientifically.
- The findings of the uncertainty budget demonstrated:
  o the influence of parameters on U-value depends on the type of wall assembly. For instance, emissivity was the most sensitive parameter in W1 (interior-insulated) while it was the third-highest coefficient for the other walls that included interior and exterior insulation.
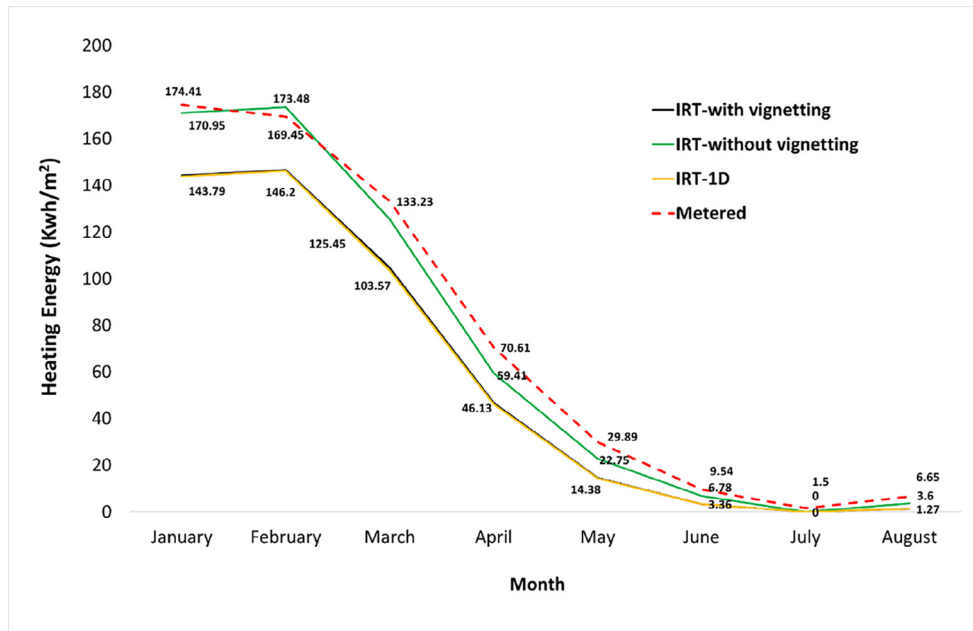
**Fig. 16.** Comparative assessment of energy models and metered energy data.

**Table 15**
Magnitude of error in simulated energy models and actual data.

| Calibration criteria | Deviations of Models | | | |
| --- | --- | --- | --- | --- |
| | 1D- IRT | IRT-with vignetting | IRT-with vingetting correction | ASHRAE Guideline 14 |
| NMBE (%) | 22.04% | 21.60% | 3.59% | ±5% |
| CVRMSE (%) | 39.30% | 38.52% | 8.93% | 15% |



**Fig. 17.** 1D U-value ROI.

**Table 16**
Comparison of calculated U-values with IRT and nominal (1D) U-values on Day 3.

| Wall | Measured 1D U-value (W/m$^2$ K) | Nominal 1D U-value (W/m$^2$ K) | Deviations (%) |
| --- | --- | --- | --- |
| W1 | 0.36 | 0.34 | 5.88 |
| W2 | 0.21 | 0.23 | −8.70 |
| W3 | 0.18 | 0.16 | 12.50 |
| W4 | 0.15 | 0.16 | −6.25 |

o surface temperature and outdoor temperature measurements with the IR camera had the largest contribution to the uncertainty of results. However, emissivity and indoor air temperature had very little impact on the uncertainty of results.

o the relatively low level of uncertainty of indoor air temperature to both U-value and IRI promotes performing external measurements with IRT without entering the building (non-invasive)

• When utilizing IRT-inferred U-values as inputs in an energy model, two criteria should be considered: (1) considering the effect of thermal bridging in the building envelope, and (2) addressing the adverse effect of vignetting. The results also were consistent with the study from Bayomi et al. [10] and Benhmidou et al. [64] where accurate estimation of U-value with IRT could enhance the accuracy of energy model calibration and selection of more appropriate retrofits for existing buildings.

Given the aspects described above, it can be concluded that the proposed methodologies may be well suited to complement other well-established techniques to better evaluate energy performance of existing buildings in Canada and beyond. Ultimately, these methodologies can help decision-makers to prioritize building envelope retrofits from a performance perspective.

Given the optimization of quantitative stationary IRT in this study, the next stage of scientific and technological advancement may involve utilizing unmanned aerial vehicles (UAVs) equipped with infrared cameras as real-time data-driven tool for conducting large-scale quantitative surveys in a fraction of the time. Also, the obtained thermal imaging data of building envelope and sensors'

data (temperature, relative humidity, and wind speed) inside/outside the building can be integrated with building information model (BIM) towards development of real-time energy audits and accurate energy simulation of buildings.

Future work should expand the viability of proposed methods for other components such as the roof or fenestration, as well as other building construction types (e.g., steel framed, concrete and mass timber buildings). Also, the reliability of the proposed methodology should be examined for various buildings types, such as office buildings in urban areas which are surrounded by different buildings (both construction and architectural aspects) and environmental objects. Finally, since the strength of the IRI approach is in its speed of analysis, the feasibility of this approach should be examined for assessing multiple buildings, for example at the neighbourhood or portfolio-levels, to ultimately rank buildings on a thermal performance basis serving as a complementary decision-making criterion for potential retrofits.

*CRediT authorship contribution statement*

**Milad Mahmoodzadeh:** Conceptualization, Methodology, Software, Investigation, Validation, Writing – original draft, Visualization, Formal analysis. **Voytek Gretka:** Conceptualization, Methodology, Validation, Visualization, Formal analysis, Writing – review & editing. **Ivan Lee:** Software, Writing – review & editing. **Phalguni Mukhopadhyaya:** Conceptualization, Supervision, Project administration, Funding acquisition, Writing – review & editing.

## Declaration of Competing Interest

The authors declare that they have no known competing financial interests or personal relationships that could have appeared to influence the work reported in this paper.

## Acknowledgment

## References

[1] BC's Greenhouse Gas Reduction Targets Act, Government of British Columbia, 2007, available at: http://www.bclaws.ca/EPLibraries/bclaws_new/document/ID/freeside/00_07042_01 (Accessed on 23 September 2021).

[2] Canada's Mid-century Long-term Low-greenhouse Gas Development Strategy, Government of Canada, 2016, available at: http://unfccc.int/files/focus/longterm_strategies/application/pdf/canadas_mid-century_long-term_strategy.pdf (Accessed on 23 September 2021).

[3] 2050 Low-carbon Economy – Climate Strategies and Targets, European Commission, 2016, available at: https://ec.europa.eu/clima/policies/strategies/2050_en (Accessed on 23 September 2021).

[4] https://www.iea.org/reports/heating-and-cooling-strategies-in-the-clean-energy-transition (Accessed on 23 September 2021).

[5] M. O'Grady, A.A. Lechowska, A.M. Harte, Quantification of heat losses through building envelope thermal bridges influenced by wind velocity using the outdoor infrared thermography technique, Appl. Energy 208 (2017) 1038–1052.

[6] International Energy Agency (IEA), Technology Roadmap "Energy Efficient Building Envelopes, 2014. doi:10.1787/9789264118492-en.

[7] O. Osama et al., Zero energy university buildings energy performance evaluation of faculty of architectural engineering, Arch. Plan. J. 23 (2015) 13–21.

[8] Y.-H. Lin, K.-T. Tsai, M.-D. Lin, M.-D. Yang, "Design optimization of office building envelope configurations for energy conservation, Appl. Energy. 171 (2016) 336–346.

[9] C.A. Balaras, K. Droutsa, A.A. Argiriou, D.N. Asimakopoulos, Potential for energy conservation in apartment buildings, Energy Build. 31 (2) (2000) 143–154.

[10] N. Bayomi, S.h. Nagpal, T. Rakha, J.E. Fernandez, Building envelope modeling calibration using aerial thermography, Energy Build. 233 (2021) 110648.

[11] B. Tejedor, E. Barreira, R.M.S.F. Almeida, M. Casals, 2020, Thermographic 2D U-value map for quantifying thermal bridges in building façades, Energy Build. 224 (2020) 110176.

[12] M. Teni, H. Krstić, P. Kosiński, Review and comparison of current experimental approaches for in-situ measurements of building walls thermal transmittance, Energy Build. 203 (2019) 109417.

[13] L. Evangelisti, C. Guattari, P. Gori, R. Vollaro, In situ thermal transmittance measurements for investigating differences between wall models and actual building performance, Sustainability 7 (8) (2015) 10388–10398.

[14] B. Tejedor, M. Casals, M. Gangolells, X. Roca, Quantitative internal infrared thermography for determining in-situ thermal behaviour of façades, Energy Build. 151 (2017) 187–197.

[15] C. Meola, Infrared Thermography: Recent Advances And Future Trends, Bentham Science Publishers, Beijing, 2012.

[16] R.A. Smith, F.E. Jones, R.P. Chasmar, The detection and measurement of infrared radiation, Clarendon, Oxford, 1958.

[17] F. Luzi, M. Malcolm, L. Nanni Costa, V. Redaelli, Thermography: current status and advances in livestock animals and in veterinary medicine, Fondazione Iniziative Zooprofilattiche e Zootecniche (2013).

[18] C.A. Balaras, A.A. Argiriou, Infrared thermography for building diagnostics, Energy Build 34 (2) (2002) 171–183.

[19] E. Lucchi, Applications of the infrared thermography in the energy audit of buildings: A review, Renew. Sust. Energ. Rev. 82 (2018) 3077–3090.

[20] International Organization for Standardization. Performance of Buildings. Detection of Heat, Air and Moisture Irregularities in Buildings by Infrared Methods—Part 3: Qualifications of Equipment Operators, Data Analysts and Report Writers; ISO 6781-3:2015; ISO: Geneva, Switzerland, 2015.

[21] International Organization for Standardization. Thermal Performance of Buildings. Qualitative Detection of Thermal Irregularities in Building Envelopes. Infrared Method; UNE EN 13187:1998; ISO: Geneva, Switzerland, 1998.

[22] American Society for Testing Materials, Standard Test Method for Minimum Detectable Temperature Di_erence for Thermal Imaging Systems; ASTM E1311;, American Society for Testing Materials, West Conshohocken, PA, USA, 2004.

[23] American Society for Testing Materials. Standard Test Method for Measuring and Compensating for Reflected Ambient Temperature Using Infrared Imaging Radiometers; ASTM E1862; American Society for Testing Materials: West Conshohocken, PA, USA, 1997.

[24] RESNET—Residential Energy Services Network. RESNET Interim Guideline for Thermographic Inspections of Buildings. 2012. Available online: http://www.resnet.us/standards/RESNET_IR_interim_guidelines.pdf (Accessed on 4 October 2020).

[25] R. Madding, Finding R-values of stud frame constructed houses with IR thermography, Proceedings of InfraMation, Reno, USA, 2008.

[26] P.A. Fokaides, S.A. Kalogirou, Application of infrared thermography for the determination of the overall heat transfer coefficient (U-Value) in building envelopes, Appl. Energy. 88 (12) (2011) 4358–4365.

[27] B. Tejedor, M. Casals, M. Gangolells, Assessing the influence of operating conditions and thermophysical properties on the accuracy of in-situ measured U-values using quantitative internal infrared thermography, Energy Build. 171 (2018) 64–75.

[28] G. Dall'O, L. Sarto, A. Panza, Infrared screening of residential buildings for energy audit purposes: results of a field test, Energies. 6 (8) (2013) 3859–3878.

[29] R. Albatici, A.M. Tonelli, M. Chiogna, A comprehensive experimental approach for the validation of quantitative infrared thermography in the evaluation of building thermal transmittance, Appl. Energy. 141 (2015) 218–228.

[30] I. Nardi, S. Sfarra, D. Ambrosini, In Quantitative thermography for the estimation of the U-value: state of the art and a case study, 32nd IUT (Italian Union of Thermo-fluid-dynamics) Heat Transfer Conference, Journal of Physics, Conference Series. 547 (2014) 012016.

[31] I. Nardi, D. Paoletti, D. Ambrosini, T. De Rubeis, S. Sfarra, U-value assessment by infrared thermography: A comparison of different calculation methods in a Guarded Hot Box, Energy Build. 122 (2016) 211–221.

[32] X. Lu, A. Memari, Application of infrared thermography for in-situ determination of building envelope thermal properties, J. Build. Eng. 26 (2019) 100885.

[33] B. Tejedor, K. Gaspar, M. Casals, M. Gangolells, Analysis of the Applicability of Non-Destructive Techniques to Determine In Situ Thermal Transmittance in Passive House Façades, Appl. Sci. 10 (23) (2020) 8337.

[34] A. Kirimtat, O. Krejcar, "A review of infrared thermography for the investigation of building envelopes: Advances and prospects, Energy Build. 176 (2018) 390–406.

[35] D. Paoletti, D. Ambrosini, S. Sfarra, F. Bisegna, Preventive thermographic diagnosis of historical buildings for consolidation, J. Cult. Heritage 14 (2) (2013) 116–121.

[36] J. Goodhew , S. Goodhew , T. Auburn , P. De Wilde , A preliminary investigation of the potential for thermographic images to influence householders ' understanding of home energy consumption, in: Proc. 25th Annu. ARCOM Conf., (2009) 971–979.

[37] S. Martín Ocaña, I. Cañas Guerrero, I. González Requena, "Thermographic survey of two rural buildings in Spain, Energy Build. 36 (6) (2004) 515–523.

[38] M. Mahmoodzadeh, V. Gretka, S. Wong, T. Froese, P. Mukhopadhyaya, Evaluating Patterns of Building Envelope Air Leakage with Infrared Thermography, Energies. 13 (14) (2020) 3545.

[39] E.C. Shao, Detecting sources of heat loss in residential buildings from infrared imaging, Massachusetts Institute of Technology, 2011, PhD diss.

[40] M. Mahmoodzadeh, V. Gretka, A. Blue, D. Adams, B. Dallimore, P.h. Mukhopadhyaya, Evaluating thermal performance of vertical building envelopes: Case studies in a Canadian university campus, J. Build. Eng. 40 (2021) 102712.

[41] T. Kalamees, Critical values for the temperature factor to assess thermal bridges, Proc. Estonian Acad. Sci. Eng. 12 (3–1) (2006) 218–229.

[42] M. Hershfield, Building Envelope Thermal Bridging Guide—Analysis, Applications and Insights (2014).

[43] S. Ilomets, T. Kalamees, Evaluation of the criticality of thermal bridges, Journal of Building Pathology and Rehabilitation 1 (1) (2016) 1–13.

[44] B.R.E. Ip, 17, 01., Assessing the Effects of Thermal Bridging at Junctions and Around Openings, BRE, Building Research Establishment Ltd, Garston (2001).

[45] NEN 2778:1991. Vochtwering in gebouwen, Bepalingsmethoden. Nederlands Normalisatieinstituut, Delft, 1991.

[46] Asumisterveysohje., Sosiaali- ja terveysministeriön oppaita 2003:1, Sosiaali-ja terveysministeriö, Helsinki (2003).

[47] Targo Kalamees, Air tightness and air leakages of new lightweight single-family detached houses in Estonia, Build Environ. 42 (6) (2007) 2369–2377.

[48] Matthew Fox, David Coley, Steve Goodhew, Pieter de Wilde, Thermography methodologies for detecting energy related building defects, Renew Sustain Energy Rev. 40 (2014) 296–310.

[49] D. González-Aguilera, S. Lagüela, P. Rodríguez-Gonzálvez, D. Hernández-López, Image-based thermographic modeling for assessing energy efficiency of buildings façades, Energy Build 65 (2013) 29–36.

[50] Itai Danielski, Morgan Fröling, Diagnosis of buildings' thermal performance-a quantitative method using thermography under non-steady state heat flow, Energy Procedia. 83 (2015) 320–329.

[51] C. Meola, G.M. Carlomagno, Recent advances in the use of infrared thermography, Measurement science and technology. 15 (9) (2004) 27.

[52] FLIR, Radiometry Application Note, May 2014

[53] E. Bauer, VP. de Freitas, N. Mustelier, E. Barreira, S. Stingl de Freitas, Infrared thermography–evaluation of the results reproducibility, Structural survey. (2015).

[54] Elton Bauer, Elier Pavón, Eva Barreira, Eliane Kraus De Castro, Analysis of building facade defects using infrared thermography: Laboratory studies, J. Build. Eng. 6 (2016) 93–104.

[55] B. Lehmann, K. Ghazi Wakili, Th. Frank, B. Vera Collado, Ch. Tanner, Effects of individual climatic parameters on the infrared thermography of buildings, Appl. Energy. 110 (2013) 29–43.

[56] Eva Barreira, Vasco P. de Freitas, Evaluation of building materials using infrared thermography, Constr Build Mater. 21 (1) (2007) 218–224.

[57] Akira Hoyano, Kohichi Asano, Takehisa Kanamaru, Analysis of the sensible heat flux from the exterior surface of buildings using time sequential thermography, Atmos Environ. 33 (24-25) (1999) 3941–3951.

[58] Rossano Albatici, Arnaldo M. Tonelli, Infrared thermovision technique for the assessment of thermal transmittance value of opaque building elements on site, Energy Build. 42 (11) (2010) 2177–2183.

[59] Milad Mahmoodzadeh, Voytek Gretka, Katie Hay, Casey Steele, Phalguni Mukhopadhyaya, Determining overall heat transfer coefficient (U-Value) of wood-framed wall assemblies in Canada using external infrared thermography, Build Environ. 199 (2021) 107897, https://doi.org/10.1016/j.buildenv.2021.107897.

[60] Małgorzata O'Grady, Agnieszka A. Lechowska, Annette M. Harte, Infrared thermography technique as an in-situ method of assessing heat loss through thermal bridging, Energy Build. 135 (2017) 20–32.

[61] Francesco Asdrubali, Giorgio Baldinelli, Francesco Bianchi, A quantitative methodology to evaluate thermal bridges in buildings, Appl. Energy. 97 (2012) 365–373.

[62] Blanca Tejedor, Eva Barreira, Ricardo M.S.F. Almeida, Miquel Casals, Automated data-processing technique: 2D Map for identifying the distribution of the U-value in building elements by quantitative internal thermography, Autom. Constr. 122 (2021) 103478, https://doi.org/10.1016/j.autcon.2020.103478.

[63] F.G.N. Li, A.Z.P. Smith, P. Biddulph, I.G. Hamilton, R. Lowe, A. Mavrogianni, E. Oikonomou, R. Raslan, S. Stamp, A. Stone, A.J. Summerfield, D. Veitch, V. Gori, T. Oreszczyn, Solid-wall U-values: heat flux measurements compared with standard assumptions, Build. Res. Inf. 43 (2) (2015) 238–252.

[64] Hajar Benhmidou, Zaid Romani, Mohamed El Mankibi, Abdeslam Draoui, Thermal performance prediction of an existing building with framing system using the IRT method, Adv. Build. Energy Res. 15 (6) (2021) 774–798.

[65] Siemens NX software, available at: https://www.plm.automation.siemens.com/global/en/products/nx/ (Accessed on 23 September 2021).

[66] A. Colantonio, G. McIntosh, The differences between large buildings and residential infrared thermographic inspections is like night and day, 11th Canadian Conference on Building Science and Technology, Banff, 2007

[67] Government of Canada, Historical Climate Data, available at: https://climate.weather.gc.ca/index_e.html (Accessed on 23 September 2021).

[68] R. Usamentiaga, P. Venegas, J. Guerediaga, L. Vega, J. Molleda, F.G. Bulnes, Infrared thermography for temperature measurement and non-destructive testing.", Sensors 14 (7) (2014) 12305–12348.

[69] Q.H. Tran, D. Han, C. Kang, A. Haldar, J. Huh, Effects of ambient temperature and relative humidity on subsurface defect detection in concrete structures by active thermal imaging, Sensors 17 (8) (2017) 1718.

[70] American Society for Testing and Materials, ASTM E1862-14, Standard Practice for Measuring and Compensating for Reflected Temperature Using Infrared Imaging Radiometers; ASTM: West Conshohocken, PA, USA, 2014.

[71] American Society for Testing and Materials, ASTM E1933-14, Standard Practice for Measuring and Compensating for Emissivity Using Infrared Imaging Radiometers; ASTM: West Conshohocken, PA, USA, 2014.

[72] N.P. Avdelidis, A. Moropoulou, Emissivity considerations in building thermography, Energy Build. 35 (7) (2003) 663–667.

[73] Katrien Maroy, Kim Carbonez, Marijke Steeman, Nathan Van Den Bossche, Assessing the thermal performance of insulating glass units with infrared thermography: Potential and limitations, Energy Build. 138 (2017) 175–192.

[74] Silvana Flores Larsen, Marcos Hongn, Determining the infrared reflectance of specular surfaces by using thermographic analysis, Renew. Energy. 64 (2014) 306–313.

[75] G. Papadakos, V. Marinakis, C. Konstas, H. Doukas, A. Papadopoulos, Managing the uncertainty of the U-value measurement using an auxiliary set along with a thermal camera, Energy Build 242 (2021) 110984.

[76] J. Kelly, N. Kljun, P.O. Olsson, L. Mihai, B. Liljeblad, P. Weslien, L. Klemedtsson, L. Eklundh, Challenges and best practices for deriving temperature data from an uncalibrated UAV thermal infrared camera, Remote Sens. 11 (5) (2019) 567.

[77] https://www.flir.com/discover/professional-tools/what-is-a-non-uniformity-correction-nuc/

[78] X. Luo, T. Hong, Y.H. Tang, Modeling thermal interactions between buildings in an urban context, Energies 13 (9) (2020) 2382.

[79] Engineering Reference — EnergyPlus 8.0, US Department of Energy, USA, 2013, https://bigladdersoftware.com/epx/docs/8-0/engineering-reference/page-020.html (Accessed on 23 September 2021).

[80] Morrison Hershfield, Thermal performance of building envelope details for mid-and high-rise buildings, ASHRAE Research Project1365-RP Final Report, 2011.

[81] ASHRAE, ASHRAE Guideline14: Measurement of Energy, Demand, and Water Savings, American Society of Heating Refrigerating and Air-Conditioning Engineers, Inc, Atlanta, Georgia, 2014.

[82] D. Patel, J Estevam Schmiedt, M. Röger, B Hoffschmidt, Approach for external measurements of the heat transfer coefficient (U-value) of building envelope components using UAV based infrared thermography, In Proceedings of the 14th Quantitative InfraRed Thermography Conference (QIRT), Berlin, Germany, 25–29 June 2018; QIRTCouncil: Berlin, Germany, (2018) 379–386.